AD_____

Award Number: W81XWH-08-1-0447

TITLE:
Respiratory Challenges in Breast Cancer: Potential for Enhanced Diagnostics and Therapy

PRINCIPAL INVESTIGATOR:

Jae G. Kim, Ph.D.

CONTRACTING ORGANIZATION:

The Beckman Laser Institute and Medical Clinic
The University of California at Irvine
Irvine, CA, 92612

REPORT DATE: July 31, 2009

TYPE OF REPORT: Annual Report (Year 1)

PREPARED FOR: U.S. Army Medical Research and Materiel Command
504 Scott Street, Fort Detrick, Maryland 21702-5012

DISTRIBUTION STATEMENT:
☑ Approved for public release; distribution unlimited

REPORT DOCUMENTATION PAGE

Form Approved
OMB No. 0704-0188

Public reporting burden for this collection of information is estimated to average 1 hour per response, including the time for reviewing instructions, searching existing data sources, gathering and maintaining the data needed, and completing and reviewing this collection of information. Send comments regarding this burden estimate or any other aspect of this collection of information, including suggestions for reducing this burden to Department of Defense, Washington Headquarters Services, Directorate for Information Operations and Reports (0704-0188), 1215 Jefferson Davis Highway, Suite 1204, Arlington, VA 22202-4302. Respondents should be aware that notwithstanding any other provision of law, no person shall be subject to any penalty for failing to comply with a collection of information if it does not display a currently valid OMB control number. **PLEASE DO NOT RETURN YOUR FORM TO THE ABOVE ADDRESS.**

1. REPORT DATE *(DD-MM-YYYY)* 31-07-2009	2. REPORT TYPE Annual Report	3. DATES COVERED *(From - To)* (1 July 2008-30 June 2009)

4. TITLE AND SUBTITLE

Respiratory Challenges in Breast Cancer: Potential for Enhanced Diagnostics and Therapy

5a. CONTRACT NUMBER

5b. GRANT NUMBER
W81XWH-08-1-0447

5c. PROGRAM ELEMENT NUMBER

6. AUTHOR(S)

Jae Gwan Kim, Ph.D.

Principal Investigator's e-mail: jaegk@uci.edu

5d. PROJECT NUMBER

5e. TASK NUMBER

5f. WORK UNIT NUMBER

7. PERFORMING ORGANIZATION NAME(S) AND ADDRESS(ES)
The Beckman Laser Institute and Medical Clinic
The University of California at Irvine
1002 Health Sciences Rd East
Irvine, CA 92612-1475

8. PERFORMING ORGANIZATION REPORT

9. SPONSORING / MONITORING AGENCY NAME(S) AND ADDRESS(ES)

U.S. Army Medical Research and Materiel Command

Fort Detrick, Maryland 21702-5012

10. SPONSOR/MONITOR'S ACRONYM(S)

11. SPONSOR/MONITOR'S REPORT NUMBER(S)

12. DISTRIBUTION / AVAILABILITY STATEMENT

Approved for public release; distribution unlimited

13. SUPPLEMENTARY NOTES

14. ABSTRACT
For the first year of this project, I took the trainings that are necessary to perform this study and have started to monitor the changes in endogenous tissue chromophores such as oxy-, deoxy-, total hemoglobin concentration, tissue oxygen saturation, lipid and water contents during tumor growth and chemotherapy using a diffuse optical imaging system that we developed at Beckman Laser Institute. We also started to monitor the changes of endogenous chromophores during chemotherapy using a spontaneous mice breast tumor model. During the optical imaging measurements, we switched a breathing gas from air to 100% oxygen and measured the changes in endogenous chromophores. Our results showed that oxy and total hemoglobin concentration increased as tumor grows and decreased when tumors regress due to chemotherapy and also showed that scattering map can help to identify tumor location. Breathing gas intervention from air to 100% oxygen increased oxyhemoglobin and decreased deoxyhemoglobin and thus increased tissue oxygen saturation. The changes during oxygen gas intervention were significantly different between chemotherapy responding tumors versus non responding tumors in the spontaneous mice breast tumor model. These results tell us that hyperoxic gas intervention can enhance the detection of tumor and also possibly predict tumor response to the treatment.

15. SUBJECT TERMS
Diffuse Optical Imaging, Tumor Angiogenesis, Chemotherapy Monitoring, Breast Cancer, Hyperoxic Gas Intervention

16. SECURITY CLASSIFICATION OF:			17. LIMITATION OF ABSTRACT	18. NUMBER OF PAGES	19a. NAME OF RESPONSIBLE PERSON: USAMRMC
a. REPORT U	**b. ABSTRACT** U	**c. THIS PAGE** U	UU	31	**19b. TELEPHONE NUMBER** *(include area code)*

Standard Form 298 (Rev. 8-98)
Prescribed by ANSI Std. Z39.18

Table of Contents

2008-2009 ANNUAL SUMMARY REPORT (YEAR 1)

This report presents the specific aims and accomplishments of our breast cancer research project during the first year of funding sponsored by the U.S. Army Department of the Defense. It covers our activities from July 1, 2008 to June 30, 2009.

INTRODUCTION

Since tumor vasculatures and metabolism are different from normal tissues (Jain, 2005; Tayek, 1992), tumor will respond to hyperoxic/hypoxic gas intervention differently. Hyperoxic gas intervention will visualize tumors from non tumors by enhancing oxygenation in tumors better than non tumors. Compare to currently available exogenous contrast materials used for MRI, PET, and Fluorescence Imaging, this hyperoxic/hypoxic gas intervention is cost effective and safe to use for human which can be easily applied to clinical trials. Tumor oxygenation also plays a key role in cancer treatment. Higher oxygenation in tumor improves the efficacy of radiation therapy (Gray *et al.*, 1953), photodynamic therapy (Henderson and Fingar, 1987), and some type of chemotherapy (Brown, 1993; Teicher *et al.*, 1981; Vaupel, 2002). Meanwhile, it has been found that other type of chemotherapeutic drugs responds better when the tumor is in hypoxic condition (Brown, 1993; Siemann *et al.*, 1991). Therefore, modulating tumor oxygenation could be used to enhance the treatment efficacy depending on the type of therapy. The goals of this research are to enhance breast cancer detection, to improve chemotherapy efficacy, and to predict tumor responses to treatments by incorporating hyperoxic/hypoxic gas interventions into non invasive optical imaging system that we have developed.

BODY

The following tasks have been proposed in our approved statement of work.

Task 1: To obtain the knowledge and appropriate training for handling tumor cells, tissue cultures and performing tumor implantation. (**months 1-4**):

a.   Write an animal protocol for this study and get an approval (month 1-3)

b.   Get training for tissue culture at biochemistry lab at BLI (month 1).

c.   Get training for tissue histology/immunohistochemistry at histology lab at BLI

d.   Study the fundamentals and operation of the laser speckle imaging (months 1-2).

e.   Get training for tumor implantation on a rat mammary fat pad model. (months 2-3).

f.   Get training for surgical installation of dorsal skin fold window chamber on rodents (months 3-4).

Task 2: To monitor changes of tissue components during tumor growth using a modulated imaging (MI) system. (**months 5-12**):

a. To order Fisher 344 rats (n=154) for this task. (month 5-12)

b. To implant breast tumors on mammary fat pad of Fisher 344 rats. (month 5-12).

c. To perform MI measurements on breast tumors with oxygen/carbogen/hypoxic gas intervention during tumor growth. (months 5-12)

d. To perform histology/immunohistochemistry on harvested tumors. (months 5-12)

e. To compare the tissue optical composition changes with histology/ Immunohistochemical results. e(month 12)

In the first year, my focus was to obtain the appropriate knowledge and skills for conducting the project (months 1-4), and to perform the measurements of tissue components during tumor growth by using modulated imaging system. I have mainly accomplished these tasks, as reported below:

Accomplishments during the first period (months 1-4):

a. Wrote/modified animal protocols for this study and got an approval. (Protocol numbers are 2006-2639 and 2002-2340)

b. Had training for tissue culture at biochemistry lab at BLI and learned the process of histology at histology lab at BLI. I also learned immunohistochemistry procedure for CD31 antibody from Dr. Eva Lee's lab who is one of my collaborators for this study.

c. Studied the fundamentals and also operation of both modulated imaging (MI) and laser speckle imaging (LSI).

d. Had training for tumor cell inoculation into the rat mammary fat pad from Dr. Edward Nelson who is one of my collaborators for this study.

e. Had training for surgical procedure of dorsal skin fold window chamber installation on rodents from Dr. Bernard Choi who is one of my collaborators.

The principles of modulated imaging and laser speckle imaging are described below.

-Modulated Imaging (MI)

MI has the unique capability of spatially resolving optical absorption and scattering parameters, allowing wide-field quantitative mapping of tissue optical properties(Cuccia *et al.*, 2005; Bevilacqua, 2003).. While compatible with temporally-modulated photon migration methods, MI alternatively uses spatially-modulated illumination for imaging of tissue constituents. Periodic illumination patterns of various spatial frequencies are projected over a large (many cm^2) area of a sample. The reflected image differs from the illumination pattern due to the optical property characteristics of the sample. Typically, sine-wave illumination patterns are used. The demodulation of these spatially-modulated waves characterizes the sample modulation transfer function (MTF), which embodies the optical property information.

Light from a halogen lamp is expanded onto a spatial light modulator (SLM). The current system uses a Digital Micromirror Device (DMD) from Texas Instruments, a 1024 x 768 binary mirror array which generates arbitrary grayscale patterns. Such patterns are directed to the tissue surface. The diffusely reflected light is then recorded by a digital CCD camera. A liquid crystal tunable filter is used to interrogate a discrete number of wavelengths. Crossed linear polarizers can be introduced into the source and detection light paths to remove specular reflectance. The SLM, CCD and filter are synchronized with a computer, enabling fast acquisition of a series of patterns at various spatial frequencies. A schematic diagram is shown in Figure 1a. A TiO$_2$-based silicone reflectance standard is used to calibrate the source intensity and to correct for spatial nonuniformities in both the illumination and imaging systems.

A detailed description of the MI method including spatial frequency domain measurement, calibration, and analysis has been previously reported (Cuccia, 2006; Cuccia *et al.*, 2009). Here, the key concepts important for this work is outlined (Figure 1b). The tissue is illuminated with a spatial pattern of the form:

$$S = \frac{S_0}{2}\left[1 + M_0 \cos(2\pi f_x x + \alpha)\right] \qquad (1)$$

where S_0, M_0, f_x and α are the illumination source intensity, modulation depth, spatial frequency, and spatial phase, respectively. The diffusely reflected intensity, I, is a sum of AC and DC components, where the measured AC component of the reflected intensity, I_{AC}, can be modeled as $I_{AC}=M_{AC}(x,f_x)\cdot\cos(2\pi f_x+\alpha)$. Here, $M_{AC}(x,f_x)$ represents the amplitude of the reflected photon density "standing wave" at frequency f_x. Note that M_{AC} can be a function of position, x.

(a)

(b)

(c)

(d)

Figure 1. MI methodology summary. a) MI platform. b) Flowchart of data processing: Intensity data at each frequency (three phase images per frequency) are amplitude demodulated, calibrated, and fit. Data are processed separately for each pixel, generating spatial maps of optical properties. Similarly, phase data (c) provide topology information which can be used for correction of curvature-related illumination nonuniformities. d) Schematic of modulated illumination source and the resulting modulated internal fluence rate.

To obtain $M_{AC}(x,f_x)$, we employ a simple time domain amplitude demodulation method (Carlson, 1988; Neil *et al.*, 1997), illuminating a sinusoid pattern three times at the same spatial frequency, with phase offsets $\alpha = 0$, $2/3\pi$ and $4/3\pi$ radians. $M_{AC}(x,f_x)$ can then be calculated algebraically at each spatial location, x_i, by $M_{AC}(x,f_x)=[(I_1-I_2)^2+(I_2-I_3)+(I_3-I_1)]^{1/2}$, where I_1, I_2, and I_3 represent the I_{AC} image values at each location with shifted spatial phases. The spatially-varying DC amplitude, $M_{DC}(x)$, can be calculated

at any frequency of illumination using $M_{DC}(x,f_x)=[I_1+I_2+I_3]/3$. Finally, measurement of a reference turbid phantom of known optical properties allows model-based calibration for the source intensity, S_0, and therefore conversion of M_{AC} and M_{DC} to calibrated diffuse reflectance, R_{AC} and R_{DC}, respectively. In a similar algebraic fashion, the spatially-varying phase can be measured, yielding topological data about the 3D tissue surface (Figure 1c).

Figure 1d depicts the diffuse propagation of a normally-incident, periodically-varying plane wave source with spatial frequency f_x and spatial phase α, giving rise to a diffuse fluence rate with the same frequency and phase. The behavior of these waves can be described by a 1-D second-order Helmholtz equation for the fluence rate as a function of depth, z:

$$\frac{d^2}{dz^2}\varphi_0(z) - \mu_{eff}'^2\varphi_0(z) = -3\mu_{tr}q_0(z) \tag{2}$$

where $\mu_{eff}' = [\mu_{eff}^2+(2\pi f_x)^2]^{1/2}$, Φ_0 is the fluence rate, q_0 is the source, $\mu_{tr}=(\mu_a + \mu_s')$ is the transport coefficient, $\mu_{eff} = [3\mu_a\mu_{tr}]^{1/2}$, μ_a is the absorption coefficient, $\mu_s'=\mu_s(1-g)$ is the reduced scattering coefficient, and g is the cosine of the average scattering angle. The solution for the resulting diffuse fluence rate (Figure 1(d)) is

$$\varphi_0(z) = \frac{3P_0\mu_s'/\mu_{tr}}{\mu_{eff}'^2/\mu_{tr}^2 - 1}\exp(-\mu_{tr}z) + C\exp(-\mu_{eff}'z), \tag{3}$$

where P_0 is the source intensity and C is determined by the choice of a boundary condition. Using the partial current boundary condition (Haskell *et al.*, 1994)**,** the diffuse reflectance, R_d, is given by:

$$R_d(k) = \frac{3A\mu_s'/\mu_{tr}}{\left(\mu_{eff}'/\mu_{tr}+1\right)\left(\mu_{eff}'/\mu_{tr}+3A\right)}, \tag{4}$$

where A is a proportionality constant from boundary conditions at the air-tissue boundary, and μ_{eff}' is a function of both optical properties and spatial frequency of illumination (Cuccia, 2006; Neil *et al.*, 1997).

-Laser Speckle Imaging (LSI)

Noninvasive blood flow imaging can provide critical information on the state of biological tissue and the efficacy of approaches to treat disease. Laser Doppler flowmetry and laser Doppler imaging have been applied in numerous preclinical and clinical studies on the brain(Dunn *et al.*, 2001; Sheth *et al.*, 2005), retina(Ferguson *et al.*, 2004; Riva *et al.*, 2005), skin(Forrester *et al.*, 2004; Boignard *et al.*, 2005), and joints(Egan *et al.*, 2004). A primary limitation of these methods is the need for mechanical scanning of the probe laser beam, resulting in long (on the order of min) image collection times. A method for high spatial and temporal resolution imaging of blood flow dynamics is required to provide objective evaluation of external stimuli, such as pharmacological intervention, electrical stimulation, or laser irradiation.

In 1981, Fercher and Briers(Fercher and Briers, 1981) proposed a laser speckle imaging (LSI) approach as an alternative to laser Doppler imaging. This method employs quantitative, spatially resolved analysis of the speckle pattern that is observed within images of laser irradiated objects. The speckle phenomenon is due to electromagnetic wave interference effects that result essentially in both spatial and temporal modulation of the imaged reflectance pattern. On the basis of this study, it was concluded that variations in speckle contrast can be used to provide directly a wide-field velocity distribution map.

7

With laser doppler imaging, temporal intensity fluctuations of each speckle (or a collection of speckles) is monitored at high sampling frequencies (on the order of MHz). An increase in fluctuation frequency is associated with faster blood flow. In contrast, LSI relies on acquisition and analysis of a single image captured at an exposure time that is considerably longer than a characteristic correlation time associated with the fluctuation frequency. A faster blood flow appears more blurred in the captured image than regions of slower or no flow. The degree of blurring is quantified as the local speckle contrast value (see Equation 5 below), with zero contrast representing no speckle and hence high blood flow, and unity contrast representing a fully developed speckle pattern and hence no flow.

Based on laser speckle statistics, Fercher and Briers derived the following relationship between the speckle contrast (K) and the normalized autocorrelation function of the remitted light:

$$K^2 = \sigma^2 / \langle I \rangle^2 = (1/T)\int_0^T |\gamma(t)|^2 \, dt \tag{5}$$

where σ is the variance, $\langle I \rangle$ is the mean and T is the integration time of the time-averaged speckle image, and $\gamma(t)$ is the normalized autocorrelation function of the remitted light. For a Lorentzian velocity distribution:

$$|\gamma(t)| = \exp(-|t|/\tau_c), \tag{6}$$

where τ_c is the correlation time. Substitution of Eq. 6 into Eq. 5 yields the following Eq. 7:

$$K = \left\{ (\tau_c/2T)\left[1 - \exp(-2T/\tau_c)\right] \right\}^{1/2} \tag{7}$$

For $T/\tau_c > 2$, corresponding to K values of 0 to 0.6, Eq 7 can be simplified to the following algebraic expression:

$$\tau_c = 2TK^2 \tag{8}$$

Accomplishments during the second period (months 5-12):

a. We obtained quantitative changes in endogenous chromophores such as oxy-, dexoy-, total hemoglobin, lipid, water, and tissue oxygen saturation from rat breast tumor on Fisher 344 rats during its growth and also during chemotherapy using cyclophosphamide.

b. We applied wide-field function imaging system to our rat tumor model to estimate tumor oxygen consumption rate during tumor growth.

c. In addition to our proposed task during months 5-12, we had a chance to image mice breast tumors with oxygen intervention during chemotherapy. (**proposed in Task 4 (month 15-24)**)

- Endogenous Optical Signals Changes in Rat Mammary Breast Tumor during Its Growth

Once animals had enough time to adapt themselves in a new environment after their arrival (> 3days), we inoculated one millions of 13762 MAT-III tumor cells in the right caudal mammary fat pad of female Fisher 344 rats (~160g) and the contralateral mamma served as control. We acquired diffuse optical images before tumor cell inoculation as a baseline or day 0 and acquired images daily for 5 days using MI system. MI system acquired the raw images from the breast tissue surface by projecting the four spatial frequency patterns of NIR light with wavelengths from 650 to 980 nm at every 10nm. From the raw images, the quantification of oxy- ([HbO$_2$]), deoxy- ([Hb]), total [HbT] hemoglobin, tissue oxygen saturation (S_tO_2(%)=[HbO$_2$]/[HbT] X 100), and water contents as well as the light scattering were carried out.

During five days of tumor growth, there was a very slight decrease of animal's body weight possibly due to daily anesthesia for about an hour, but not significant. (Figure 2a) We couldn't measure tumor volume until day 3 and after then ellipsoidal volume approximation was used to estimate tumor volume. (Figure 2b) (Tumor volume = $4/3*\pi*a*b*c$ where a and b are the equatorial radii (along the x and y axes) and c is the polar radius (along the z-axis))
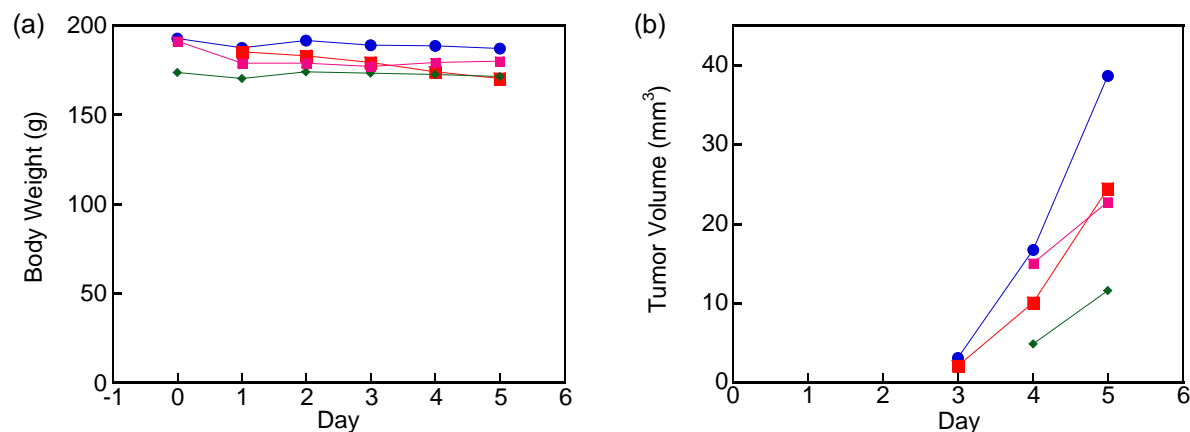

Figure 2. The changes of body weight (a) and tumor volume during 5 days after tumor cell inoculation.

Figure 3. Color photos showing the development of tumors after inoculation. One million of 13762 MAT-III rat mammary tumor cells were inoculated in the right caudal mammary fat pad. The tumor growth became visible at day 4. Pink dotted line represents field of view of images.

Figure 3 shows the visual tumor growth after tumor cells inoculation. Tumor growth became obvious at day 3 on the right side of the field of view. Once we collect raw reflectance images at different spatial frequencies with the wavelength range from 650 to 980nm at every 10nm, raw images are demodulated and then the reflectance intensity is fitted using Eq. 4 to estimate absorption and scattering properties of tissues. (Figure 4)
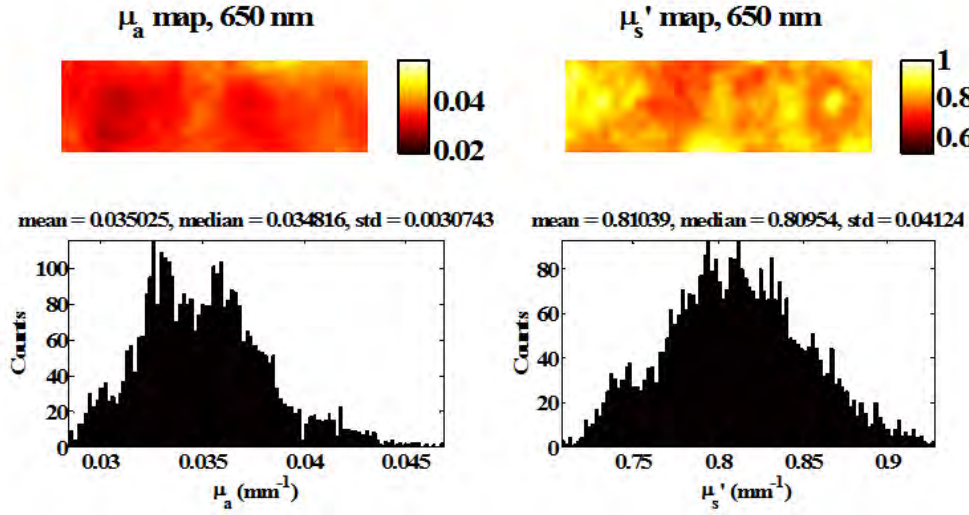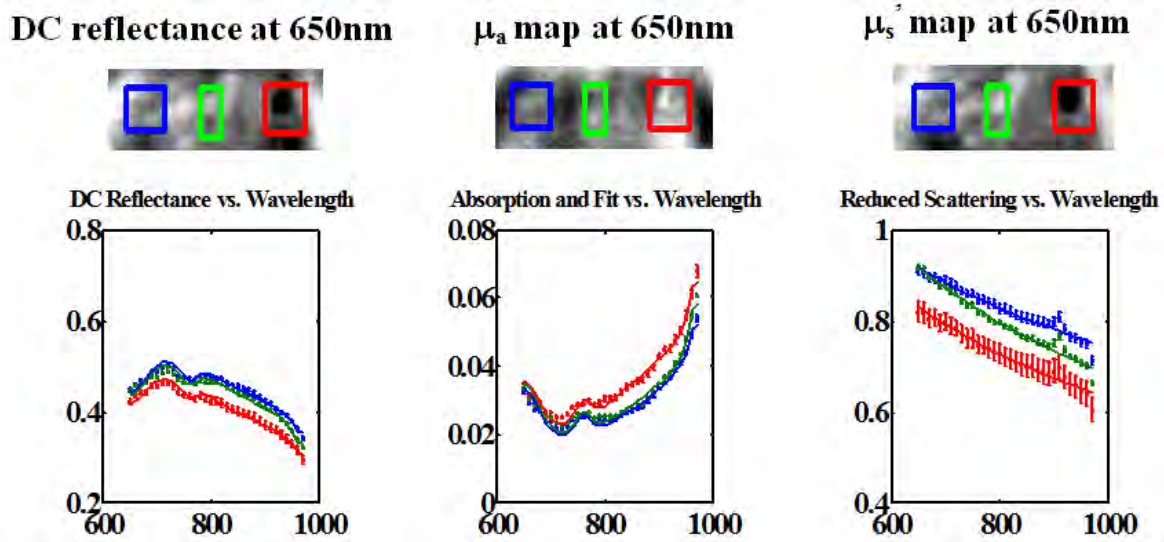

Figure 4. The absorption and scattering map at 650nm with the histogram are shown.

Figure 5. DC reflectance (left), absorption (middle), and reduced scattering (right) spectra from three regions of interest colored by blue(contralateral mamma), green (middle of abdomen), and red (tumor).

Once we obtain absorption and scattering properties of tissue at each wavelength, we can then have absorption and scattering spectra shown below. (Figure 5) These spectra already show the difference between tumor and non tumor region. Tumor was selected by red box and the resulting reflectance,

absorption, and scattering spectra are shown as red lines while those spectra from contralateral mamma are shown as blue lines. It shows that tumor has higher absorption but lower scattering than non tumor.

Table 1. The estimated concentration/percentage of chromophores from the three regions of interest in Figure 5.

Chromophores	Region1 (Blue)	Region2 (Green)	Region3 (Red)
HbO_2 (μM)	71.5	73.5	99.5+_ SD
Hb (μM)	29.9	31.5	29.5
HbT (μM)	101.4	105	129
S_tO_2 (%)	70.5	70	77
Lipid (%)	31.2	26.4	24.4
Water (%)	58	69.3	68.2

Table 1 summarizes the concentration/percentage of endogeneous chromophores in three regions. Tumors, region 3, have higher oxyhemoglobin (HbO_2) and total hemoglobin (HbT) than non tumor, region 1 and 2 which means a high activity of angiogenesis occurring in tumors.
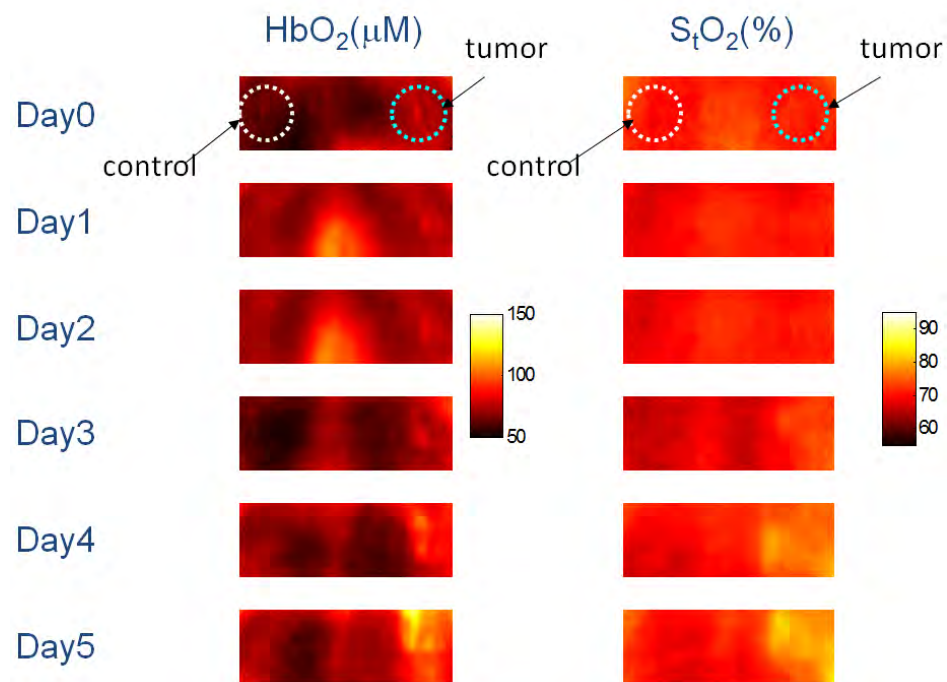

Figure 6. Changes of oxyhemoglobin (HbO2) and tissue oxygen saturation (StO2) during 5 days of tumor growth.

In Figure 6 we can see clearly that tumor site has more oxygenated hemoglobin and thus higher tissue oxygen saturation that contralateral side possibly presenting an active angiogenesis of tumors.

We also compared the scattering map among days of tumor growth. The scattering spectra (Figure 5) can be fitted with power law equation (Reduced Scattering = $A*wavelength^{-B}$) and found that A and B maps can show tumor growth much earlier than that by visual inspection as shown in Figure 7.
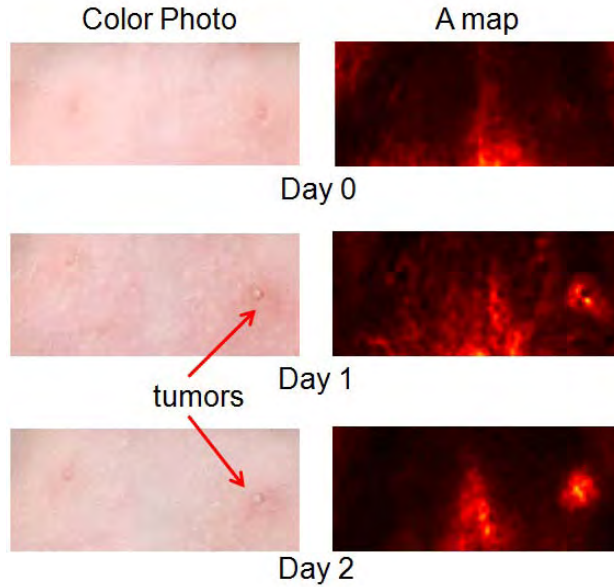

Figure 7. Color photos on the left and A map from reduced scattering fitting by power law are shown on the right before and 2 days after tumor cell inoculation.
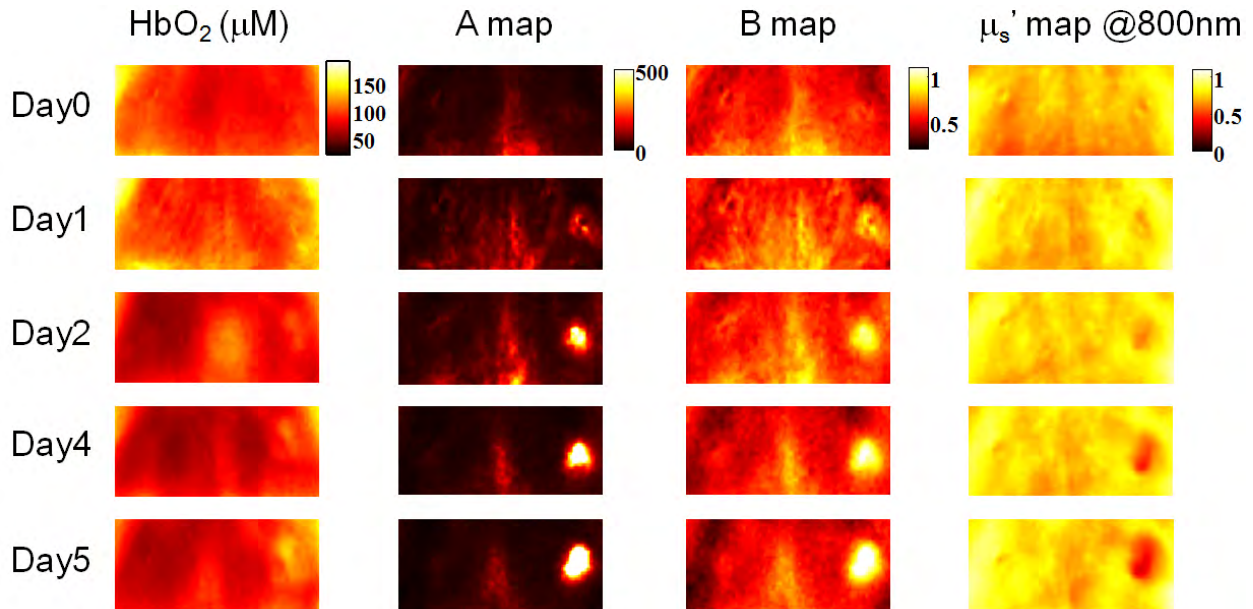

Figure 8. Changes of oxyhemoglobin, A, B, and reduced scattering map after tumor cell inoculation. A and B maps show the clear boundary of tumors even at day 1.

12

Figure 8 s hows representative images during 6 da ys of tumor growth after one million of tumor cell inoculation. Although oxyhemoglobin also shows the existence of tumor in the right side at day 2, A and B maps clearly show us the location of tumors even at day 1.

Averaged changes of each chromophore are shown in Figure 9. During tumor growth, both oxy and total hemoglobin concentration increased while deoxyhemoblogin concentration didn't. This implies there is an increase of tumor oxygen consumption because deoxyhemoglobin should decrease when oxyhemoglobin increases if oxygen consumption rate is same. Increase of total hemoglobin was mainly from the increase of oxyhemoglobin which means there is a very active formation of new blood vessels. As a result, tissue oxygen saturation increased in tumors compared to non tumors. Interestingly, lipid content decreased while water content increased as tumors grow.
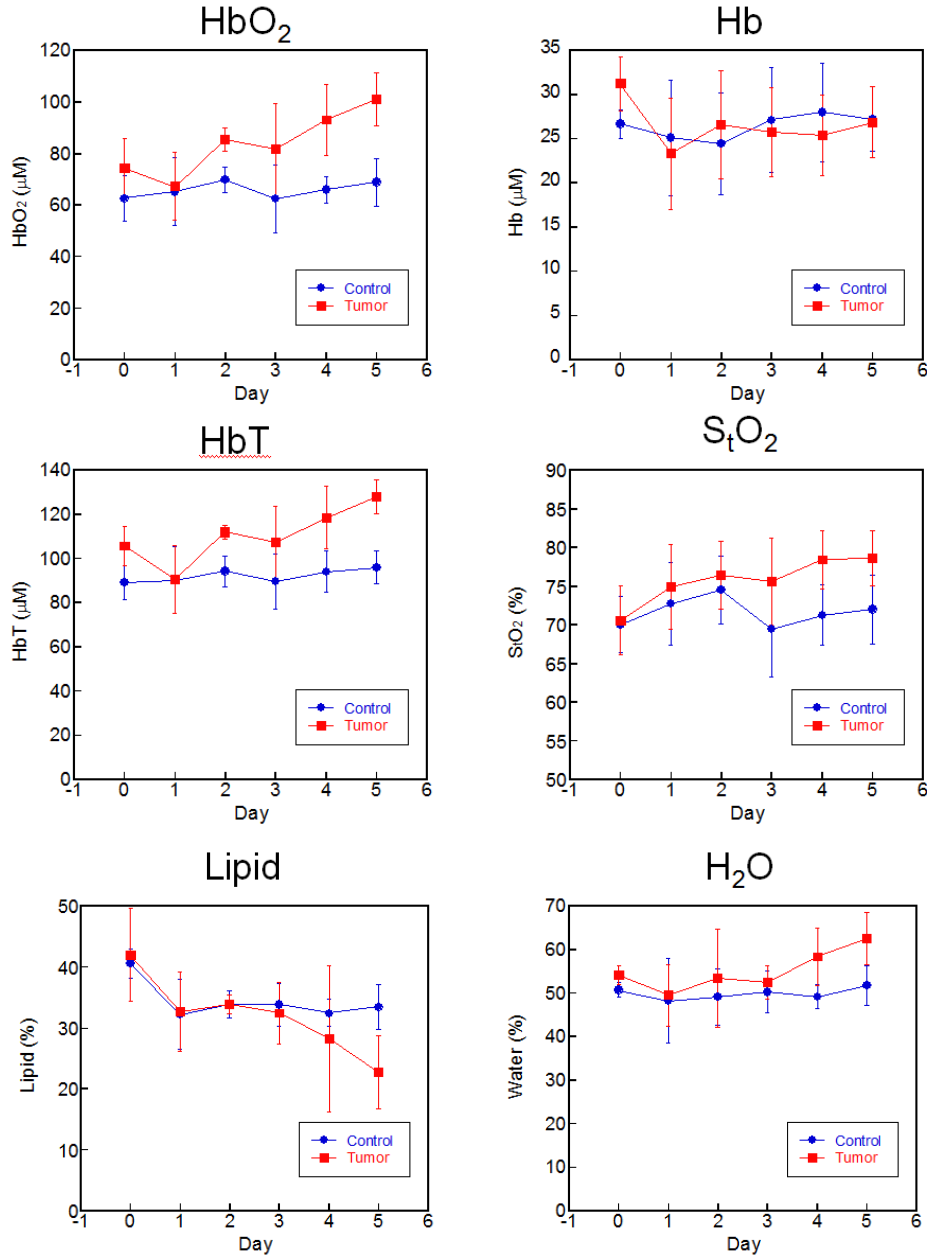

Figure 9. Chromophore changes during tumor growth. Red lines represent tumors and blue lines represent the changes from contralateral mammae.

With the help from Dr. Edward Nelson's lab, we stained frozen tumor tissue sections with two different types of antibodies to visualize blood vessels in tumors. The first one we tried was using CD31(or PECAM-1, platelet endothelial cell adhesion molecule) shown at the top of Figure 10. The other is RECA-1 (endothelial cell antibody) and stained tissue images are shown at the bottom of Figure 10. Both CD31 and RECA-1 staining show the blood vessels in the sectioned tissues, but RECA-1 appears to be a little better in terms of contrast to show the blood vessels in tumors.
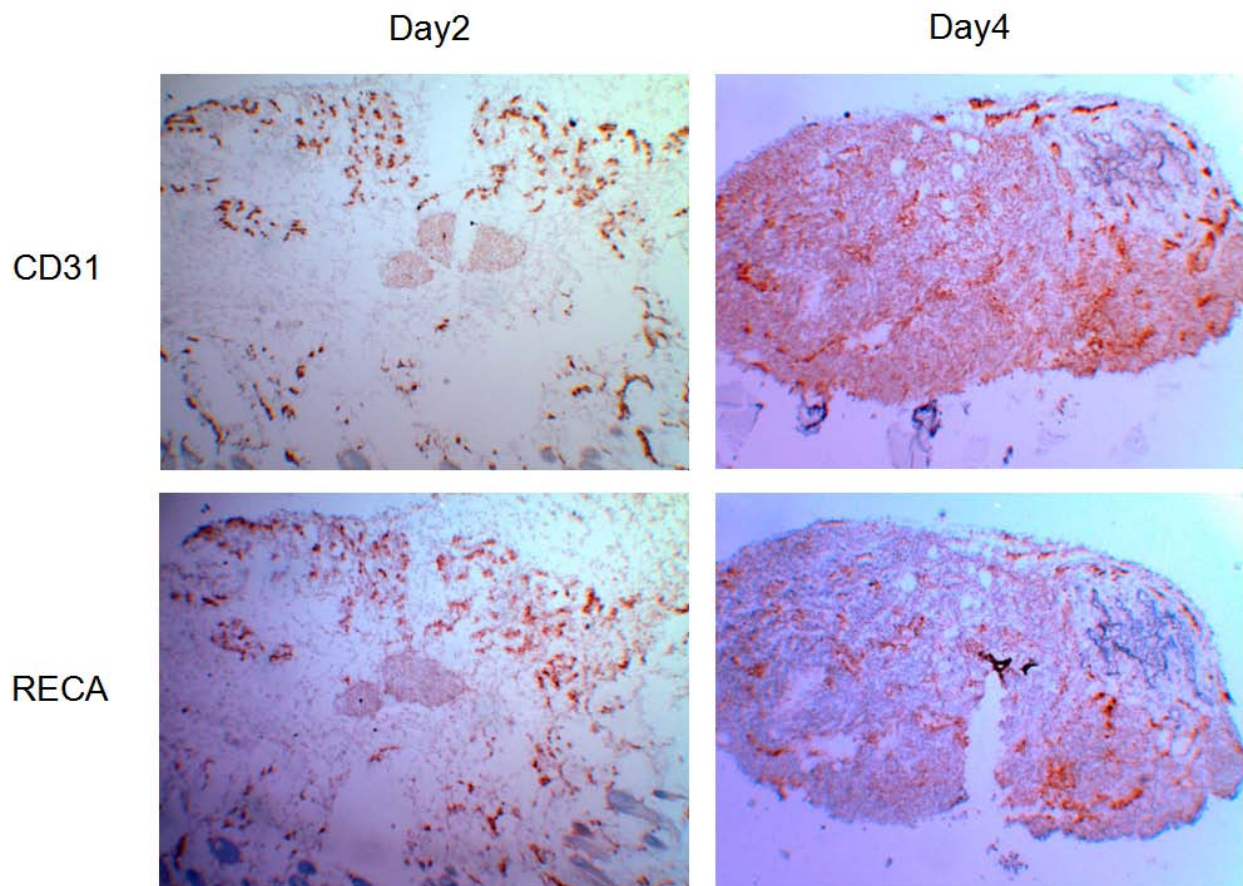

Figure 10. Tumor tissues stained with CD31 (top) and RECA-1 (bottom) at day2 (left) and at day4 (right).

At day2, two clusters of tumor cells can be seen in the center of the images from both CD31 and RECA-1 stained images, and there are blood vessels surrounding tumor cells possibly representing the initiation of angiogenesis toward tumor cells. At day 4, tumors have grown so big and now we can see the heterogeneous formation of blood vessels inside the tumors while some necrotic area can be seen. From Figure 8, we showed that scattering map can locate tumors earlier than oxyhemoglobin map which is from the absorption information. Figure 10 supports those by showing that tumors don't have many blood vessels at day 2 but are well vascularized at day 4 which means the scattering changes can be seen even at day 2 but absorption changes can be detectable when tumors grow to a certain volume.

- Endogenous Optical Signals Changes in Rat Mammary Breast Tumor during Chemotherapy

We used the same animal model described in the previous section for this chemotherapy study. Basically, we inoculated tumor cells in the mammary fat pad of Fisher 344 rats (~160g) and waited for its growth.

Once the diameter of tumors becomes about 1cm in diameter, 20mg/kg of cyclophosphamide (CTX) was administered by i. p. injection every other day for 10 days (total dose = 100mg/kg) and modulated imaging was taken during and post chemotherapy. Body weight didn't change much during and post chemotherapy, but we could see the significant reduction in tumor volume from 13762MAT-III tumors but not from R3230AC tumors. (Figure 11)
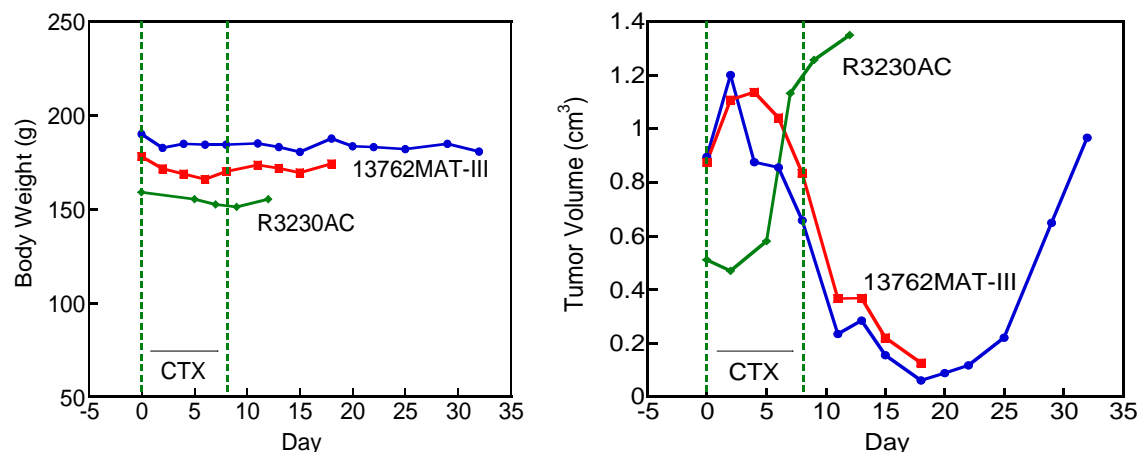

Figure 11. The changes of body weight and tumor volume during and post chemotherapy using cyclophosphamide.
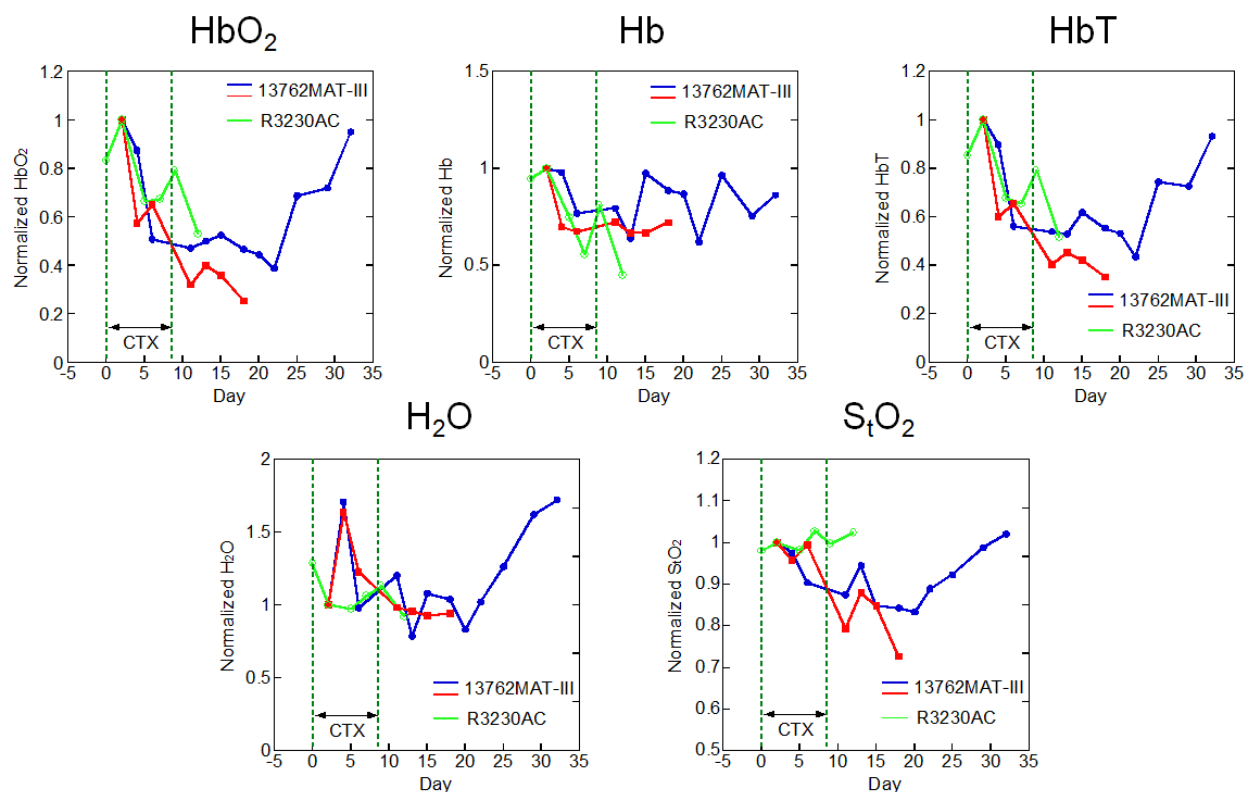

Figure 12. Normalized changes of each chromophore concentration/percentage during cyclophosphamide treatment and post treatment.

As we mentioned earlier, 13762MAT-III tumors responded to cyclophosphamide treatment while R3230AC tumor didn't. Oxy (HbO_2), deoxy (Hb), and total (HbT) hemoglobin concentration decreased during CTX treatment from both 13762MAT-III and R3230AC tumors, however, tissue oxygen saturation (S_tO_2) was maintained for the R3230AC but decreased for 13762MAT-III tumors.
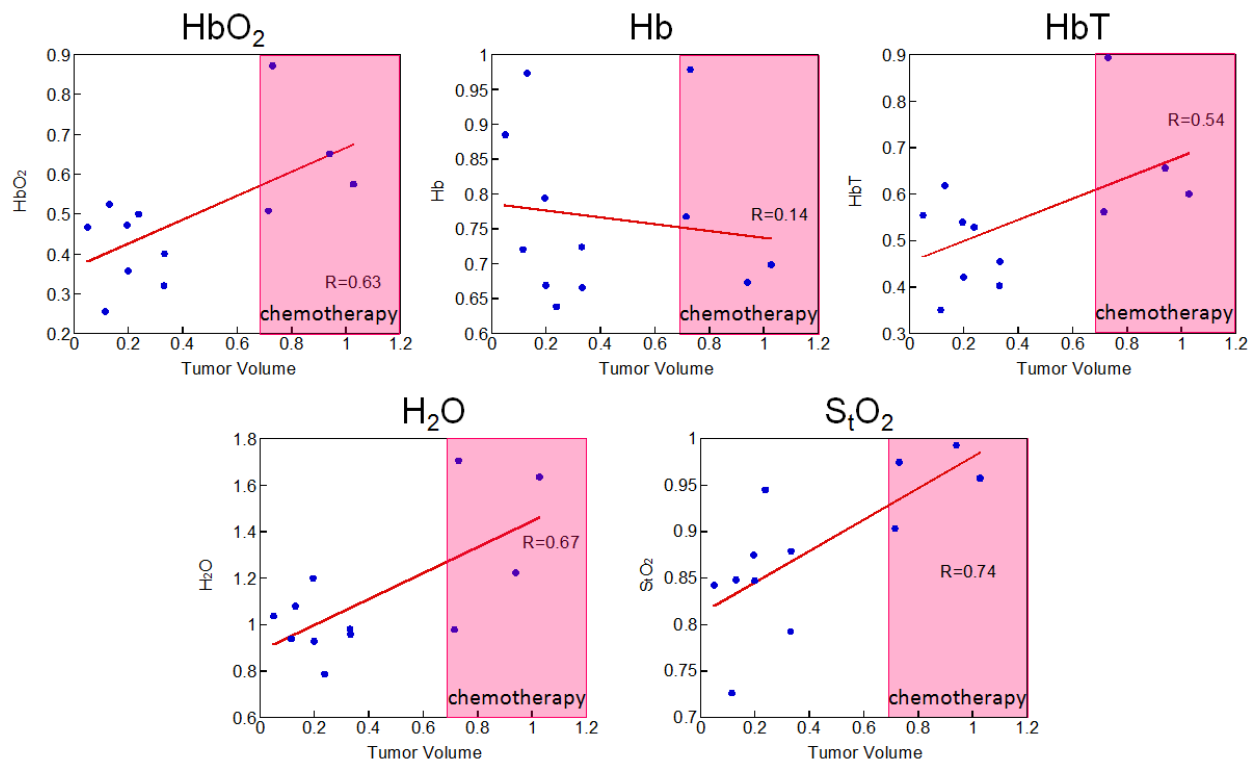

Figure 13. Correlation plots of each chromophore concentration versus tumor volume changes during and post chemotherapy.
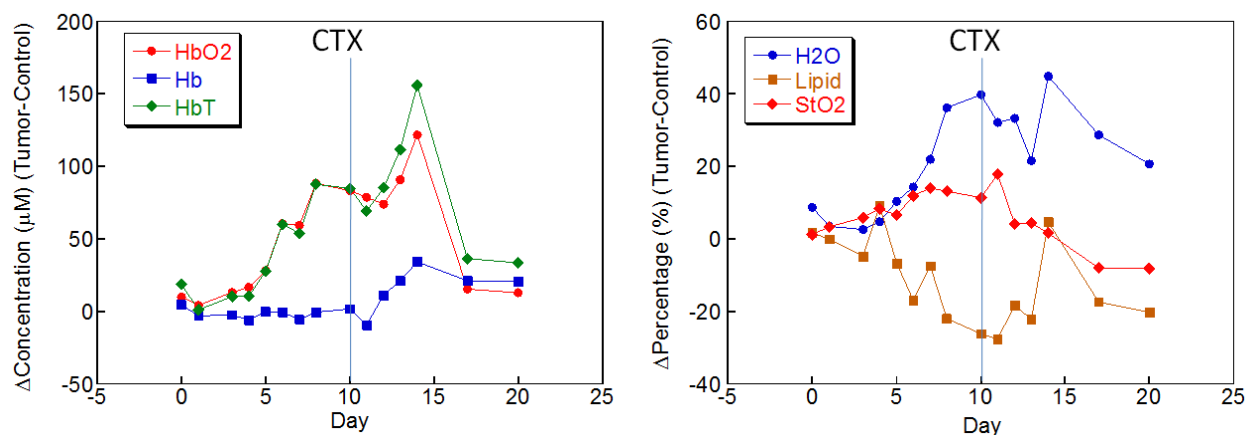

Figure 14. Another representative data of chromophores concentration change during tumor growth and during chemotherapy.

For the CTX responded tumors, we plotted chromophore concentration changes versus tumor volume changes. (Figure 13) Most of them are pretty well correlated to the changes in tumor volumes. Decrease of oxyhemoglobin, total hemoglobin, water content, and tissue oxygen saturation were observed as

tumors regress while deoxyhemoglobin didn't change much although there seems slight increase of deoxyhemoglobin when tumors are small. Another case of changes in chromophore concentration during tumor growth and chemotherapy is shown in Figure 14. During tumor growth, oxy and total hemoglobin, water, tissue oxygen saturation increased then reversed post CTX treatment. In this case, CTX was given as a single high dose (100mg/kg) at day 10. The trends of each chromophore concentration during tumor growth and chemotherapy are consistent with the previous results.

-Monitoring tumor oxygen consumption rate change during tumor growth by using a Wide Field Function Imaging (WiFI) System

The benefit of combining modulated imaging (MI) system with laser speckle imaging (LSI) system is that it enables us to estimate mammary metabolic rate of oxygen (MMRO$_2$) by measurement of deoxyhemoglobin (ctHHb) and total hemoglobin (ctTHb) form MI and blood flow index (BFI) from LSI by using an Eq. 9 (Zhou *et al.*, 2007)

$$\text{MMRO}_{2(T/N)} = \frac{\gamma_T}{\gamma_N} \cdot \frac{\text{ctHHb}_T}{\text{ctHHb}_N} \cdot \left(\frac{\text{ctTHb}_T}{\text{ctTHb}_N} \right)^{-1} \cdot \frac{\text{BFI}_T}{\text{BFI}_N}, \tag{9}$$

where T and N represent the values for tumor and normal breast tissue i.e., normal tissues within the same breast, and $\gamma_{T(N)}$=[ctHHbv$_{T(N)}$ /ctTHbv$_{T(N)}$] /[ctHHb$_{T(N)}$/ctTHb$_{T(N)}$] is the ratio of tumor or normal deoxy-to-total-hemoglobin in the venous compartment (v) compared to the ratio of deoxy-to total-hemoglobin in the total vasculature. The simplest approximation, which we adopt here, assumes the ratio of γ_T/γ_N to be 1 and constant over time.

We first obtained MI and LSI images from each imaging system, but soon realized the difficulties of coregistration and consistency of imaging setup parameters. Therefore, we combined two systems by incorporating LSI laser source into our current MI system as shown in Figure 15. We now then take both MI and LSI images from one system and one animal setup which enable us to coregister images from MI and LSI system.
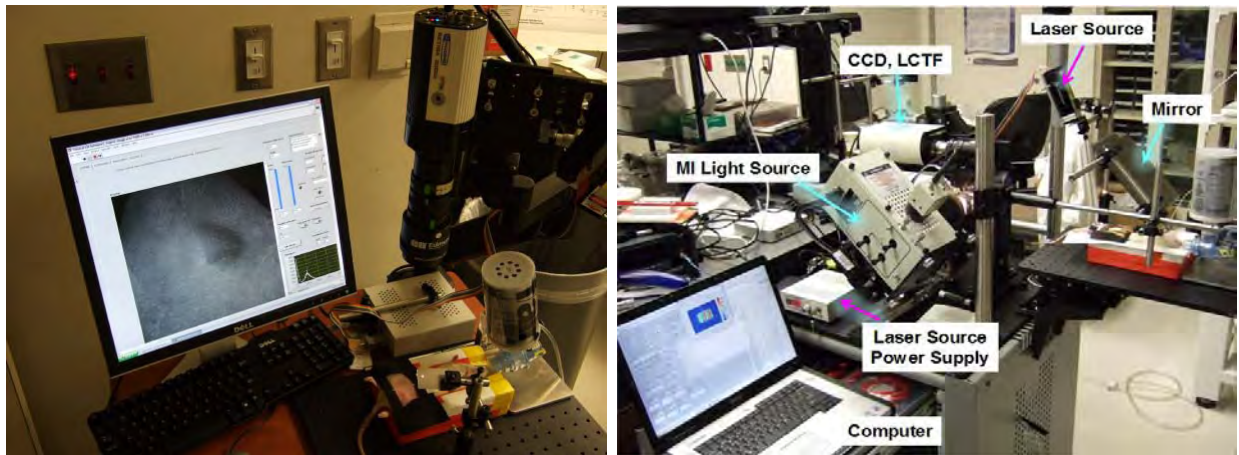

Figure 15. Photos of laser speckle imaging system (left) and combined MI and LSI system (right).

Tumor cells were inoculated as described earlier in this report but at this time to the left side of caudal mamma and color photos of tumor growth are shown in Figure 16. Tumors become visible at day 3 and partial necrosis occurred at day 5. Changes of chromophore concentration and speckle flow index during 6 days post tumor cell inoculation are shown in Figure 17.
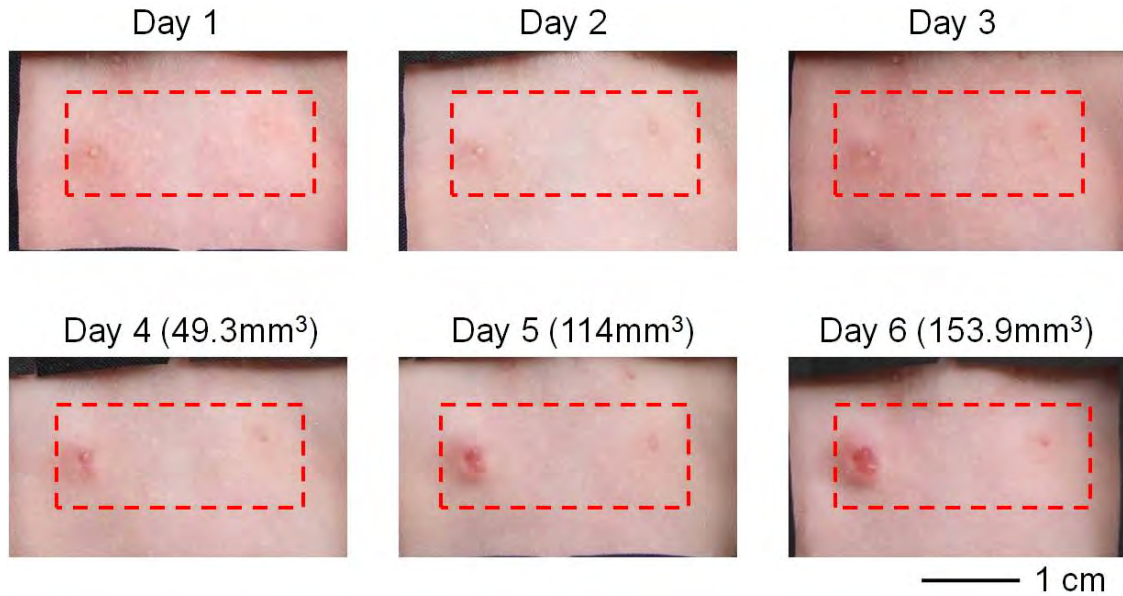

Figure 16. Color photos of tumor growth in the left side of field of view.
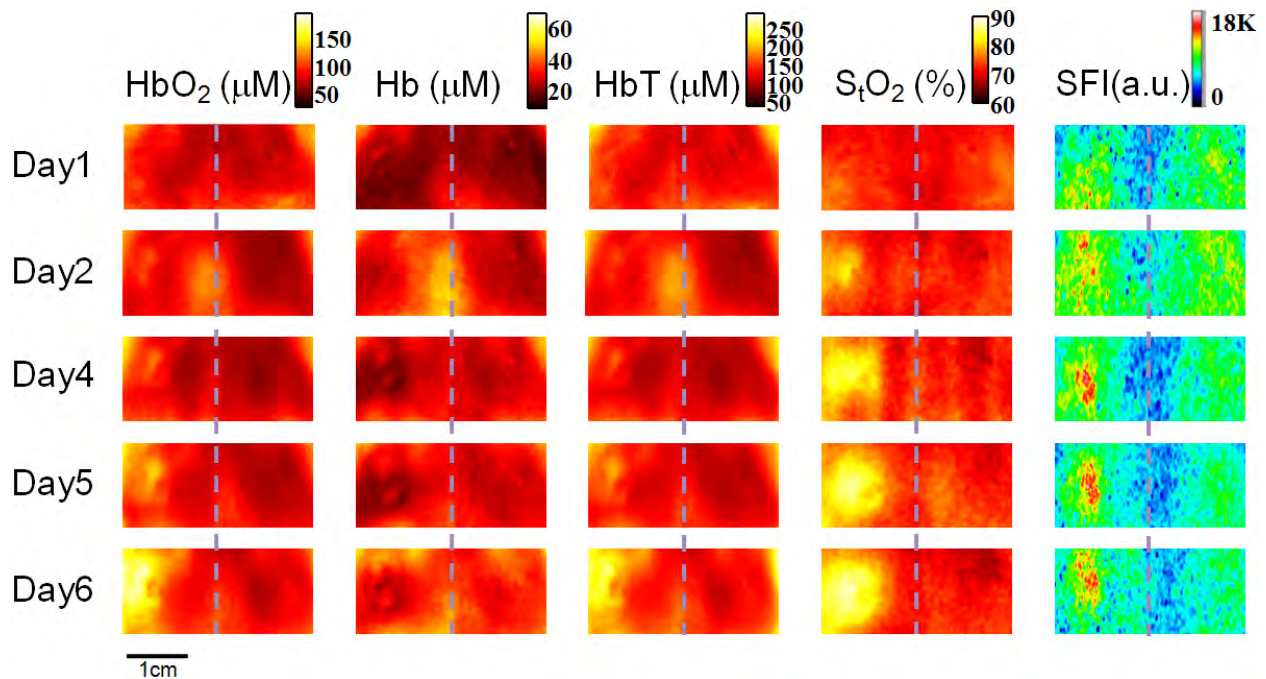

Figure 17. Chromophores concentration and speckle flow index (SFI) are shown during 6 days after tumor cell inoculation.

Oxyhemoglobin (HbO2), total hemoglobin (HbT), and tissue oxygen saturation (StO2) increased in tumors compared to normal contralateral mamma while deoxyhemoglobin (Hb) slightly decreased during 6 days of tumor growth which is consistent with the results shown earlier in this report. (Figures 9 and 14)
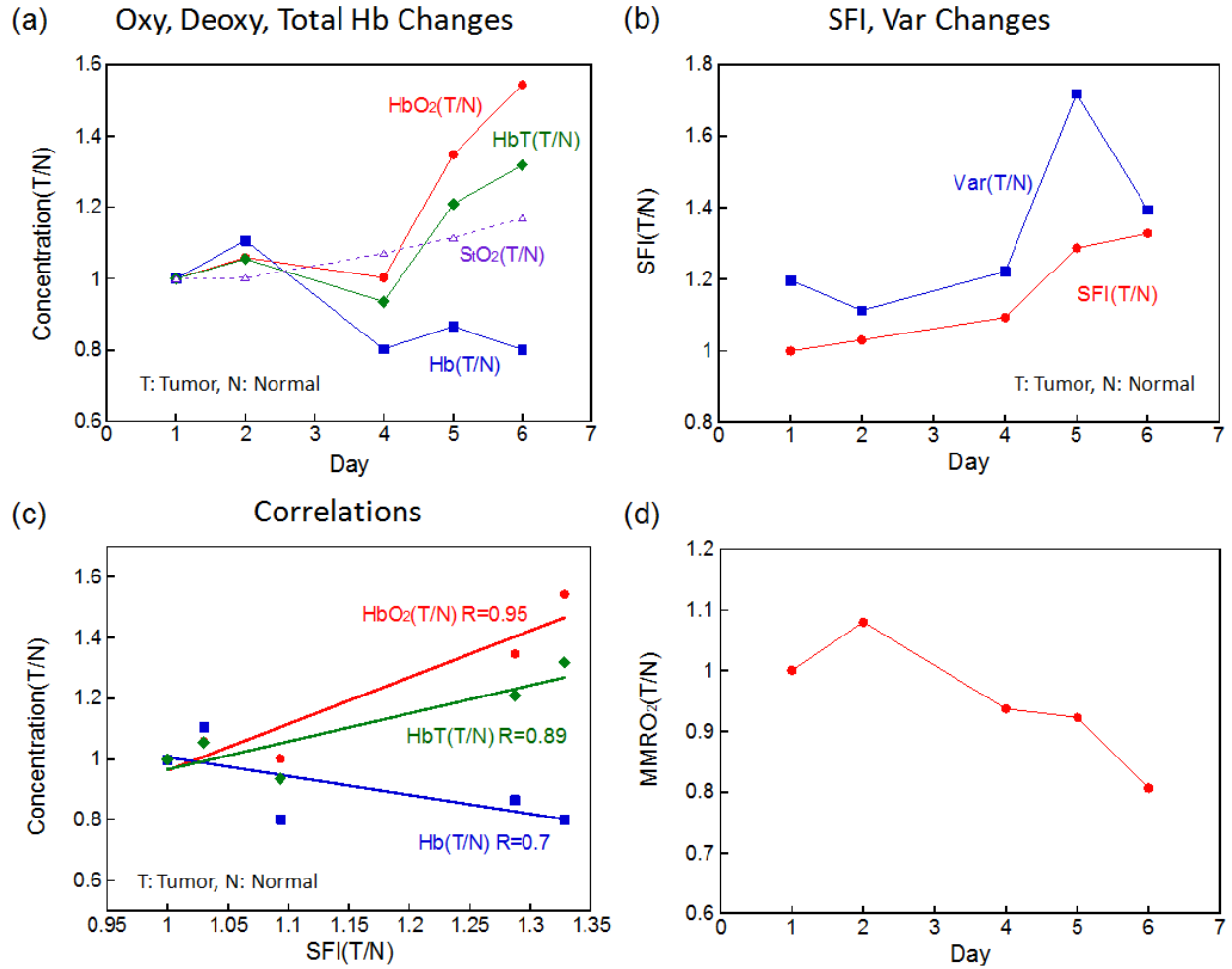

Figure 18. Summary plots from WiFI measurement. (a) The normalized tumor oxy-(HbO_2), deoxy-(Hb), total (HbT) hemoglobin concentration changes to the contralateral mamma during tumor growth, (b) The normalized speckle flow index (SFI) and variance within region of interest (Var) changes as tumor grows, (c) Correlations between SFI and HbO2, Hb, and HbT, (d) mammary metabolic rate of oxygen ($MMRO_2$) changes as tumor grows.

Figure 18 summarizes the results from WiFI measurement during 6 days of tumor growth. All the data are normalized by dividing values in tumors with values in contralateral mamma. Figure 18a confirms our previous findings that oxy and total hemoglobin concentration increases as tumors grow while deoxyhemoglobin concentration decreases. Speckle flow index increases as tumors grow indicating the increase of blood flow in tumors. Variance within region of interest also increases as tumor grows which implies the vascular structure of tumor becomes more and more heterogeneous so that there are greater variance of blood flow within tumors. (Figure 18b) The correlations between SFI and HbO_2 and between SFI and HbT are positive which means tumors are having increase of blood flow as well as increase of blood volume mainly from arterial blood increase. Mammary metabolic rate of oxygen ($MMRO_2$) was estimated using Eq. 9 and the results are shown in Figure 18d. $MMRO_2$ initially increase at day 2, but then decreased as tumors grow possibly due to the formation of necrotic tissues in tumors.

-The Effects of Oxygen Intervention in Scattering and Absorption of Tissues

We hypothesized in our proposal that *Hyperoxic/hypoxic gas interventions cause more changes of oxygenation in tumors than in non-tumors.* To test our hypothesis we switched breathing gas from normal air (21% O_2) to 100% O_2 and monitored changes of scattering and absorption properties of tissues. (Figure 19)
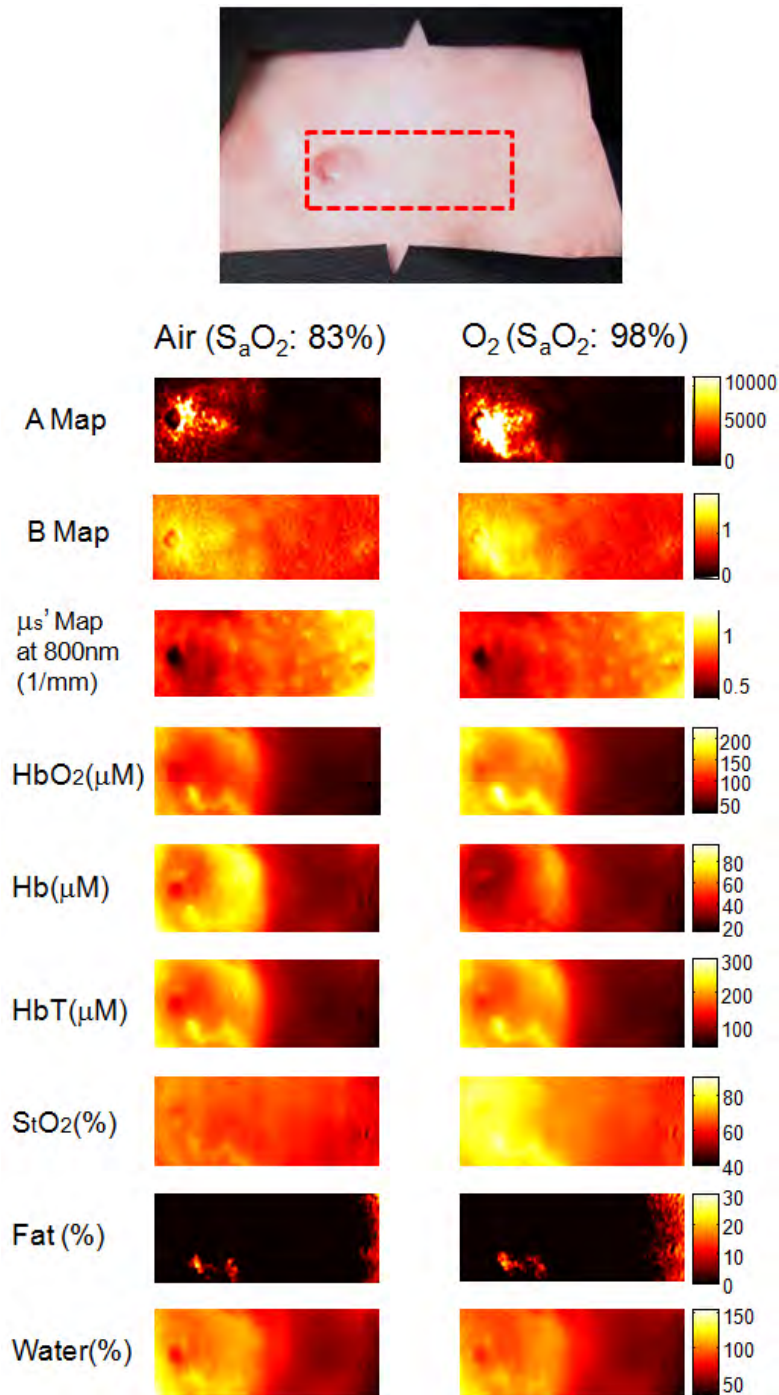

Figure 19. 100% oxygen intervention effects on scattering and the concentration of endogeneous chromophores.

A breathing gas switch from air to 100% oxygen caused an increase of A and B values of power law fitting of scattering (reduced scattering = A*wavelength^{-B}). It also increased oxyhemoglobin (HbO$_2$), but decreased deoxyhemoglobin (Hb), and thus resulted significant increase of tissue oxygen saturation (S$_t$O$_2$). However, total hemoglobin concentration (HbT) value did not change much which is consistent with little change in reduced scattering at 800nm since 800nm is close to the isosbestic point of oxy and deoxyhemoglobin absorption. Fat and water content were also not changed much during oxygen intervention.

Figure 20. 100% oxygen intervention effects on the concentration of HbO$_2$, Hb, HbT, and S$_t$O$_2$ from tumors and non tumors.

Figure 20 is a time plot showing the changes of oxy, deoxy, total hemoglobin concentration during oxygen gas intervention from tumors (red) and contralateral mamma (black) from another animal. Unlike the total hemoglobin change shown in Figure 19, we can see a drop of total hemoglobin in tumors and this tells us how the vascular function of tumor differs among tumors themselves.

-Hyperoxic respiratory challenges to monitor chemotherapy effects on Brca1/p53 deficient mice breast tumors.

Response to cancer treatments such as radiotherapy, chemotherapy, and photodynamic therapy are less effective when tumors are hypoxic. Hyperoxic gas intervention has been shown to improve tumor oxygenation. Here we report how hemodynamic changes due to oxygen intervention are related to the tumor response during cisplatin treatment of spontaneous mammary tumors developed in mice with conditional inactivation of the Brca1 and p53 genes.

We treated mammary tumors in Brca1/p53 knockout mice (n=8) with 1.2mg/kg of Cisplatin (i. p. daily for a week), and tumor volume and body weight were monitored during treatment. We imaged tumors during chemotherapy using an optical imaging system that quantifies intrinsic light scattering and absorption by projecting spatially modulated, near infrared (NIR) light (650nm to 980nm) onto tissues and calculating oxy-(OHb), deoxy-(RHb), total hemoglobin (HTb) concentrations, tissue oxygen saturation (S_tO_2) values, and scattering values at all wavelengths. During imaging, animals were anesthetized using 1.5% isoflurane and each animal inhaled medical air (33% O_2) for 6 min followed by 100% oxygen for an additional 12 min.
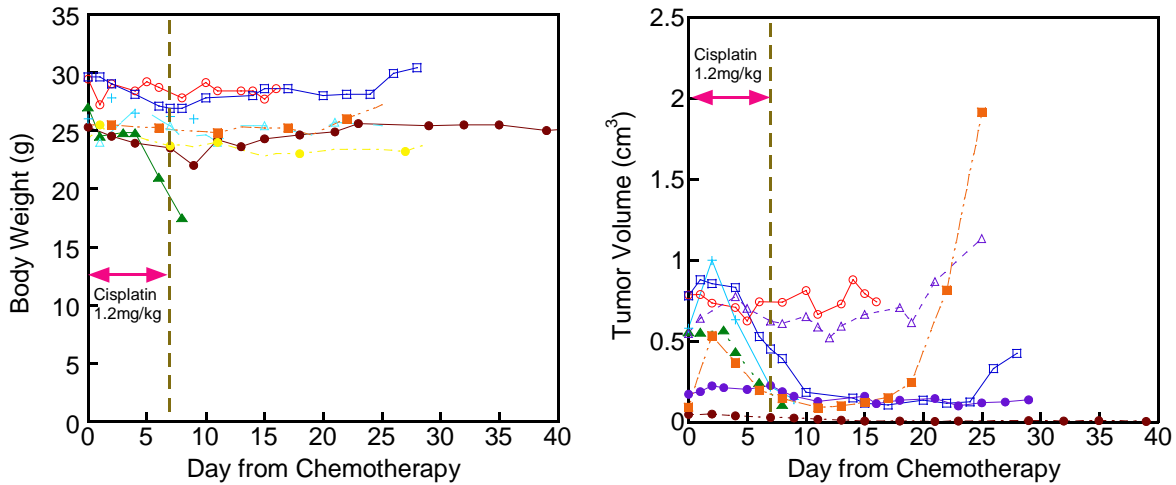

Figure 21. The changes of body weight and tumor volume during and post cisplatin treatment.

Most of animals under cisplatin treatment did not show a significant loss of body weight. Among 8 tumors, 5 (volume=0.38±0.1) showed response to Cisplatin treatment while the other 3 tumors (volume=0.56±0.12) did not. (Figure 21) The representative data from responding and non-responding tumors are shown in Figure 22. Figure 22 a and c are showing tumor volume changes during cisplatin treatment and b and d are showing the difference of oxy-(HbO$_2$), deoxy-(Hb), and total (HbT) hemoglobin concentrations between oxygen breathing and air breathing. Therefore, positive values of Δ[HbO$_2$] in this plot means [HbO$_2$] increased by oxygen breathing. Again, negative values of Δ[Hb] in the graph implies that deoxyhemoglobin decreased by switching breathing gas from air to oxygen. These differences became smaller as tumors responded to cisplatin treatment and got larger as tumors grow back. Meanwhile, non responding tumors did not show the changes of Δ[HbO$_2$] or Δ[Hb] during the treatment and post treatment of cisplatin.

We compared the changes in concentration from air inhalation to oxygen inhalation between cisplatin responding and non responding group at day 0 meaning prior to cisplatin treatment. The results are shown

in Figure 23. Tumors responding to cisplatin displayed greater than 2-fold increase in $[HbO_2]$ and $[Hb]$ during oxygen intervention compared to non responding tumors ($p<0.05$). (Figure 23)
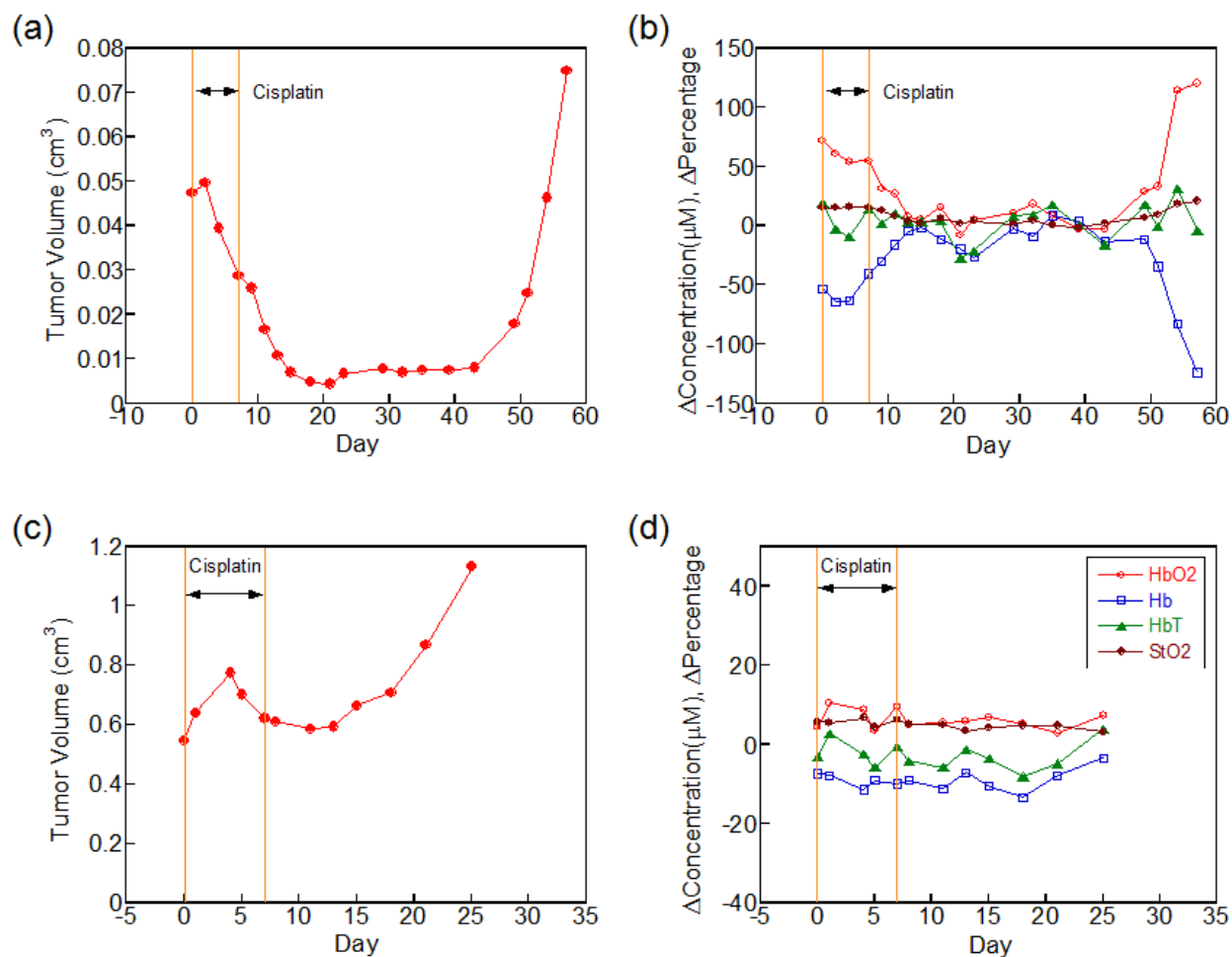

Figure 22. The representative data from responding (a and b) and non responding (c and d) tumors during cisplatin treatment.
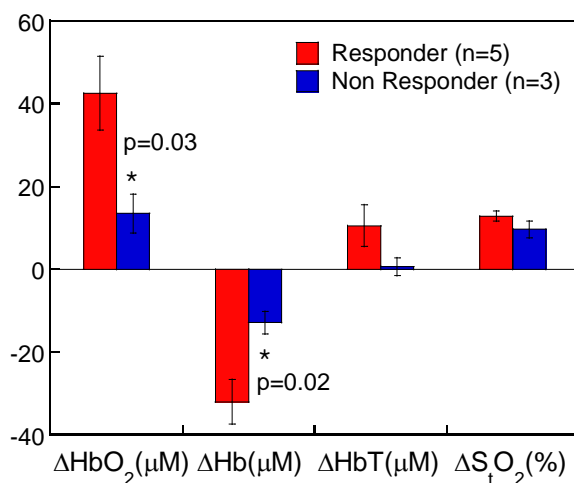

Figure 23. Comparison of changes in OHb, RHb, THb, and S_tO_2 during oxygen intervention between Cisplatin responding tumors and non responding tumors. Data are shown as mean ± standard errors.

Significant differences in tumor size changes were also observed between responders and non-responders.

Breast cancers are heterogeneous in their molecular profiles as well as treatment response. Hyperoxic gas intervention during chemotherapy combined with intrinsic signal optical imaging can be used to evaluate vascular reactivity. Our preliminary results indicate that HbO_2 and Hb reactive tumors are significantly more likely to respond to cisplatin chemotherapy. This general approach can be extended to other tumor therapy models and can be readily translated to patients.

Key Research Accomplishments:

a. Obtained the main knowledge and skills for conducting this project. (had training for tissue culture, histology, immunohistology, tumor cell inoculation, surgical procedure of dorsal skin fold window chamber installation, and studied the fundamentals and also operation of both modulated imaging (MI) and laser speckle imaging (LSI))

b. Found that monitoring endogenous tissue chromophores such as oxy and total hemoglobin concentration can visualize the tumor formation even at 2 days after tumor cell inoculation. Scattering information can also used to locate tumors from the surround tissues and looks better than oxy- or total hemoglobin in term of tumors detectability.

c. Our non invasive imaging technique confirmed the tumor angiogenesis during its growth and showed oxy and total hemoglobin increased as tumors grow. It also showed that oxy and total hemoglobin concentration decrease when tumors respond to chemotherapy.

d. We combined MI and LSI system so that we can obtain all the information required to estimate oxygen consumption rate in tumors.

e. Switching from air to 100% oxygen gas breathing caused an increase of oxyhemoglobin and a decrease of deoxyhemoglobin much greater than non tumors which can be possibly used as a contrast to find tumors from surrounding tissues.

f. 100% oxygen intervention may be able to serve as a prognostic tool whether tumors will respond to the treatment or not. We found that chemotherapy responding tumors show more than 2 folds changes of oxy and deoxyhemoglobin concentration by switching breathing gas from air to 100% oxygen compared to non responding tumors.

Reportable Outcomes

Manuscripts for Peer-reviewed Journals:

1) Jae G. Kim, Edward L. Nelson, Albert E. Cerussi, Bruce J. Tromberg, "Optical Monitoring of Tumor Angiogenesis by Modulated Imaging: Preliminary Results from In Vivo Rat Tumor Model," *In preparation.*

2) Jae G. Kim, Austin Moy, Eva Lee, Albert E. Cerussi, Bruce J. Tromberg, "Can hyperoxic gas challenge predict tumor response to chemotherapy?" *In preparation.*

Proceeding papers:

1) Austin Moy, **Jae G. Kim**, Eva YHP Lee, Bruce Tromberg, Albert Cerussi, Bernard Choi, "Brca1/p53 Deficient Mouse Breast Tumor Hemodynamics During Hyperoxic Respiratory Challenge Monitored by A Novel Wide-field Functional Imaging (WiFI) System, *Proc. SPIE-Int. Soc. Opt. Eng.*, **7174**, 71742L1-5, (2009)

Presentations:

1) **Jae G. Kim**, Yoon Kim, Albert Cerussi, Eva YHP Lee, Bruce J. Tromberg, "Hyperoxic respiratory challenges to monitor chemotherapy effects on Brca1/p53 deficient mice breast tumors", presented at San Antonio Breast Cancer Symposium, San Antonio, Texas, December 10-14, 2008

2) Austin Moy, **Jae G. Kim**, Eva YHP Lee, Bruce Tromberg, Albert Cerussi, Bernard Choi, "Application of a novel wide-field functional imaging (WiFI) instrument to a preclinical study of breast cancer progression and response to therapy", presented at International Biomedical Optics Symposium (SPIE's BIOS 2009), San Jose, California, January 24-28, 2009

3) **Jae G. Kim**, Edward L. Nelson, Eva YHP Lee, Albert Cerussi, and Bruce Tromberg, "New approaches of respiratory challenges as a con trast for cancer detection, a booster for therapy and a predictor for therapy efficacy: preclinical to clinical trial", Department of Defense The Leading Innovation and Knowledge Sharing (LINKS) meeting, Vienna, VA, Feb 9-10, 2009

Research Opportunities:

Two graduate students (Clifford Hom and Austin Moy) had research opportunities from this project. They were helping us to take images using MI and LSI system and to analyze the data.

Conclusions

From the work that I have conducted up-to-date, the following conclusions can be drawn.

Modulated imaging can quantitatively and non-invasively monitor the tissue optical properties changes during tumor growth and chemotherapy. During tumor growth, an increase of blood volume (total hemoglobin concentration) was observed and it was mainly from an increase of oxygenated hemoglobin. This implies that tumors have very active new blood vessel formation to have more supply of oxygen and nutrients from the surrounding tissues. This formation of blood vessels was also confirmed by CD31 and RECA-1 immunostaining of tumor tissue sections at different time points. When tumors responded to chemotherapy, there were decreases of oxy- and total hemoglobin concentration in tumors. In terms of tumor detectability, endogenous contrast such as A and B from power law fit of scattering were powerful to locate tumors even though oxy and total hemoglobin concentrations were also good markers to find tumors from surrounding tissues. 100% oxygen intervention caused increase of oxyhemoglobin and decrease of deoxyhemoglobin and the increase/decrease amount can be possibly served as a prognostic factor whether tumors will respond to chemotherapy or not in a spontaneous Brca1/p53 knockout mice tumor model. However, these findings further need to be confirmed by increasing numbers of animals.

The measurement throughout the long period required our experimental setup to be same for each time. This became an issue since the system had to be shared for multi projects. To resolve this, we reserved system for the certain periods to do this study, but again it limited the number of animals that we can study. Our study on the spontaneous Brca1/p53 knockout mice tumor model is supposed to start during the second year of this project. However, it normally takes 5 to 6 months to have tumors grow on the mice. Therefore, we decided to perform task 4 proposed to study between months 15 and 24 whenever we can have tumor bearing mice from our collaborator Dr. Eva Lee's lab. This also prohibited us to fulfill the number of animals that we are supposed to do in the first year, but will be continued during the second year of this project.

References

Bevilacqua F, Cuccia, D., Tromberg, B.J., Durkin, A.J., 2003 "Method and apparatus for performing quantitative analysis and imaging surfaces and subsurfaces of turbid media using spatially structured illumination": US

Boignard A, Salvat-Melis M, Carpentier P H, Minson C T, Grange L, Duc C, Sarrot-Reynauld F and Cracowski J L 2005 Local hyperhemia to heating is impaired in secondary Raynaud's phenomenon *Arthritis Research & Therapy* **7** R1103-R12

Brown J M 1993 SR 4233 (tirapazamine): a new anticancer drug exploiting hypoxia in solid tumours *Br J Cancer* **67** 1163-70

Carlson A B 1988 *Communication Systems* McGraw-Hill: New York

Cuccia D J 2006 Modulated Imaging: A Spatial Frequency Domain Imaging Method for Wide-field Spectroscopy and Tomography of Turbid Media University of California, Irvine.

Cuccia D J, Bevilacqua F, Durkin A J, Ayers F R and Tromberg B J 2009 Quantitation and mapping of tissue optical properties using modulated imaging *J Biomed Opt* **14** 024012

Cuccia D J, Bevilacqua F, Durkin A J and Tromberg B J 2005 Modulated imaging: quantitative analysis and tomography of turbid media in the spatial-frequency domain *Opt Lett* **30** 1354-6

Dunn A K, Bolay T, Moskowitz M A and Boas D A 2001 Dynamic imaging of cerebral blood flow using laser speckle *Journal of Cerebral Blood Flow and Metabolism* **21** 195-201

Egan C G, Lockhart J C and Ferrell W R 2004 Pathophysiology of vascular dysfunction in a rat model of chronic joint inflammation *Journal of Physiology-London* **557** 635-43

Fercher A F and Briers J D 1981 Flow Visualization by Means of Single-Exposure Speckle Photography *Optics Communications* **37** 326-30

Ferguson R D, Hammer D X, Elsner A E, Webb R H and Burns S A 2004 Wide-field retinal hemodynamic imaging with the tracking scanning laser ophthalmoscope *Optics Express* **12** 5198-208

Forrester K R, Tulip J, Leonard C, Stewart C and Bray R C 2004 A laser speckle imaging technique for measuring tissue perfusion *IEEE Transactions on Biomedical Engineering* **51** 2074-84

Gray L H, Conger A D, Ebert M, Hornsey S and Scott O C 1953 The concentration of oxygen dissolved in tissues at the time of irradiation as a factor in radiotherapy *Br J Radiol* **26** 638-48

Haskell R C, Svaasand L O, Tsay T T, Feng T C, McAdams M S and Tromberg B J 1994 Boundary conditions for the diffusion equation in radiative transfer *J Opt Soc Am A Opt Image Sci Vis* **11** 2727-41

Henderson B W and Fingar V H 1987 Relationship of tumor hypoxia and response to photodynamic treatment in an experimental mouse tumor *Cancer Res* **47** 3110-4

Jain R K 2005 Normalization of tumor vasculature: an emerging concept in antiangiogenic therapy *Science* **307** 58-62

Neil M A A, Juskaitis R and Wilson T 1997 Method of obtaining optical sectioning by using structured light in a conventional microscope *Opt Lett* **22** 1905-7

Riva C E, Logean E and Falsini B 2005 Visually evoked hemodynamical response and assessment of neurovascular coupling in the optic nerve and retina *Progress in Retinal and Eye Research* **24** 183-215

Sheth S A, Nemoto M, Guiou M W, Walker M A and Toga A W 2005 Spatiotemporal evolution of functional hemodynamic changes and their relationship to neuronal activity *Journal of Cerebral Blood Flow and Metabolism* **25** 830-41

Siemann D W, Chapman M and Beikirch A 1991 Effects of oxygenation and pH on tumor cell response to alkylating chemotherapy *Int J Radiat Oncol Biol Phys* **20** 287-9

Tayek J A 1992 A review of cancer cachexia and abnormal glucose metabolism in humans with cancer *J Am Coll Nutr* **11** 445-56

Teicher B A, Lazo J S and Sartorelli A C 1981 Classification of antineoplastic agents by their selective toxicities toward oxygenated and hypoxic tumor cells *Cancer Res* **41** 73-81

Vaupel P, Hockel, M. 2002 Tumor hypoxia and therapeutic resistance

Zhou C, Choe R, Shah N, Durduran T, Yu G, Durkin A, Hsiang D, Mehta R, Butler J, Cerussi A, Tromberg B J and Yodh A G 2007 Diffuse optical monitoring of blood flow and oxygenation in human breast cancer during early stages of neoadjuvant chemotherapy *J Biomed Opt* **12** 051903

Brca1/p53 Deficient Mouse Breast Tumor Hemodynamics During Hyperoxic Respiratory Challenge Monitored by A Novel Wide-field Functional Imaging (WiFI) System

Austin Moy*[1,2], Jae G. Kim[1], Eva YHP Lee[3], Bruce Tromberg[1,2], Albert Cerussi[1], Bernard Choi[1,2]
[1]Beckman Laser Institute and Medical Clinic, 1002 Health Sciences Rd., Irvine, CA USA 92612;
[2]Dept. of Biomedical Engineering, University of California, Irvine, Irvine, CA USA 92697;
[3]Dept. of Developmental and Cell Biology and Dept. of Biological Chemistry, University of California, Irvine, Irvine, CA USA 92697

ABSTRACT

Current imaging modalities allow precise visualization of tumors but do not enable quantitative characterization of the tumor metabolic state. Such quantitative information would enhance our understanding of tumor progression and response to treatment, and to our overall understanding of tumor biology. To address this problem, we have developed a wide-field functional imaging (WiFI) instrument which combines two optical imaging modalities, spatially modulated imaging (MI) and laser speckle imaging (LSI). Our current WiFI imaging protocol consists of multispectral imaging in the near infrared (650-980 nm) spectrum, over a wide (7 cm x 5 cm) field of view. Using MI, the spatially-resolved reflectance of sinusoidal patterns projected onto the tissue is assessed, and optical properties of the tissue are estimated using a Monte Carlo model. From the spatial maps of local absorption and reduced scattering coefficients, tissue composition information is extracted in the form of oxy-, deoxy-, and total hemoglobin concentrations, and percentage of lipid and water. Using LSI, the reflectance of a 785 nm laser speckle pattern on the tissue is acquired and analyzed to compute maps of blood perfusion in the tissue. Tissue metabolism state is estimated from the values of blood perfusion, volume and oxygenation state. We currently are employing the WiFI instrument to study tumor development in a BRCA1/p53 deficient mice breast tumor model. The animals are monitored with WiFI during hyperoxic respiratory challenge. At present, four tumors have been measured with WiFI, and preliminary data suggest that tumor metabolic changes during hyperoxic respiratory challenge can be determined.

Keywords: Tissue optics, speckle, cancer, metabolism, transgenic, laser Doppler perfusion imaging

1. INTRODUCTION

Cells require readily available oxygen and nutrients, such as growth factors and amino acids, to survive. These components are delivered to cells by the blood via the microvasculature. Normal microvasculature is composed of mature vessels and maintained by pro- and anti-angiogenic molecules. Tumor microvasculature, by contrast, is structurally and functionally abnormal and is characterized by tortuous, dilated and saccular blood vessels that are poorly organized and have increased permeability. This results in a vascular network that has spatial and temporal heterogeneity and greatly inhibits the delivery of oxygen and macromolecule nutrients. Finally, poor oxygen delivery creates a hypoxic environment within the tumor. These hallmark characteristics of solid tumors act in concert to limit the delivery and effectiveness of both cytotoxic and molecular targeted therapies[1].

Hyperoxic respiratory challenges have been applied to enhance the efficacy of cancer treatments such as radiotherapy by increasing tumor oxygenation[2]. Due to the abnormal state of tumor vasculature, tumors show a different response from normal tissue to respiratory challenges. In this study, we monitored changes in tumor hemodynamic parameters such as blood oxygenation, blood volume, and blood perfusion during oxygen gas intervention using a novel wide field functional imaging (WiFI) system.

*amoy@uci.edu; phone: 949-824-3054; choi.bli.uci.edu

The WiFI system consists of two components: spatially modulated imaging (MI) and laser speckle imaging (LSI). MI provides information about the biochemical composition of the tissue in question while LSI provides information about blood perfusion to the tissue.

2. MATERIALS AND METHODS

2.1 Instrumentation

2.1.1 Modulated imaging

MI makes use of spatially varying patterns (i.e. sinusoidal) of broadband light that are projected onto the tissue. These patterns are projected at different intervals, or spatial frequencies. Each of these spatial frequencies is then shifted by a certain spatial offset, or phase. Depending on the spatial frequency, different depths of tissue can be interrogated; low frequency patterns probe deeper into the tissue (maximum of 5 mm) while high frequency patterns probe shallower depths of tissue. Near IR reflectance images of the tissue are then acquired from the light projected at each of the different frequency and phase combinations onto the tissue using a camera equipped with a tunable liquid crystal filter set for the NIR regime. Optical properties (absorption and reduced scattering) of the tissue can be determined by demodulating the various frequency/phase images. From these optical properties, tissue chromophore concentrations can be calculated using a diffusion-based model of light propagation in tissue[3]. The tissue chromophores include oxyhemoglobin (HbO_2), deoxyhemoglobin (Hb), total hemoglobin (THb), lipid, and water. Based on HbO_2 and Hb values, we compute oxygen saturation (S_tO_2).

2.1.2 Laser speckle imaging

LSI utilizes temporal changes in the speckle pattern of coherent laser light to detect changes in blood perfusion. We irradiate tissue with a low-power diode laser (785 nm) and reflectance images of the speckle pattern are acquired. The reflectance, or raw speckle, image is then converted to a speckle contrast image with a sliding window operator. Finally, a speckle flow index (SFI) map, computed from the contrast image, provides tissue perfusion information. We have employed LSI to study blood flow dynamics of the rodent dorsal window chamber model[4] as well as application in the clinic in assessing port wine stain treatment[5].

2.2 Animal model

A p53/Brca1 knockout murine model developed by Dr. Eva Lee's lab was used. This model develops spontaneously occurring transgenic breast tumors[6]. Animals had tumors of sufficient size that were observed by visual inspection and were between 8-12 months of age at the start of the study.

2.3 Experimental protocol

Animal subjects were continuously measured using WiFI during medical grade air inspiration and subsequent 100% oxygen challenge. Medical air inspiration duration was eight min in duration and subsequent 100% oxygen inspiration was 20 min. The total measurement time was 28 minutes.
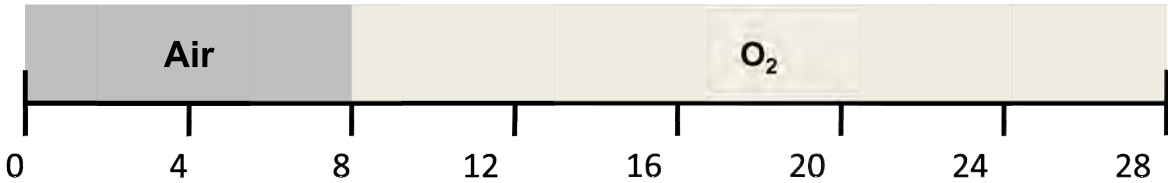

Figure 1: Diagram of experimental protocol detailing inspiration time of each gas

3. DATA

Below is a table of the changes in the pertinent tissue chromophores HbO_2, Hb, and THb, and functional parameters S_tO_2, and SFI, during a respiratory challenge.
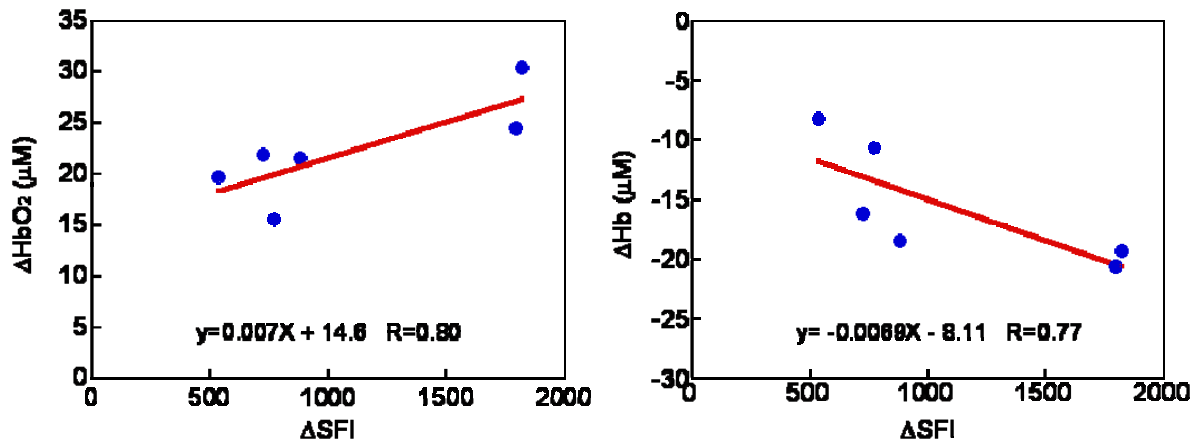
Table 1. Change in tissue chromophores and functional parameters measured with WiFI during a hyperoxic challenge. Data are from six separate measurements on different days of study.

Day	ΔHbO_2 (μM)	ΔHb (μM)	ΔTHb (μM)	ΔS_tO_2 (%)	ΔSFI
12	24.43	-20.627	3.8	12.169	1794
17	19.7	-8.23	11.46	5.741	535
19	30.45	-19.296	11.15	11.599	1818
24	21.58	-18.438	3.14	10.239	880
26	21.84	-16.172	5.07	9.169	723
28	15.5	-10.678	4.82	6.639	772

The mammary metabolic rate of oxygen ($MMRO_2$)[7] is a parameter that we used to describe the oxygen metabolism of the tumor during oxygen challenge. It is based on the total hemoglobin concentration, deoxyhemoglobin concentration, and blood perfusion values measured during air and oxygen inspiration. The parameter is defined as:

$$MMRO_2(O_2/Air) = \frac{Hb(O_2)}{Hb(Air)} \times \frac{THb(Air)}{THb(O_2)} \times \frac{SFI(O_2)}{SFI(Air)}$$

Below are plots of the change in each of the tissue chromophores against the change in SFI value. These plots give information about the relationship between the change in blood perfusion and the change in chromophore concentration.
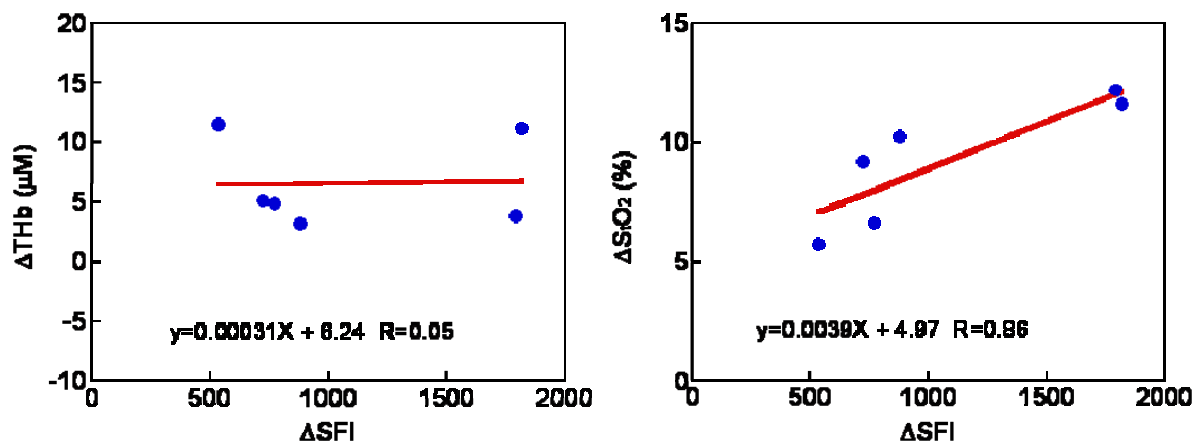
Figure 2: Plots of the changes in oxyhemoglobin (HbO_2), deoxyhemoglobin (Hb), total hemoglobin (THb), and oxygen saturation (S_tO_2) against the change in speckle flow index (SFI)

Measurement of the tissue chromophore values during air inspiration and oxygen challenge allows for calculation of the $MMRO_2$ during air inspiration and oxygen challenge. Figure 3 below shows the average change over six measurements in HbO_2, Hb, THb, S_tO_2, SFI, and $MMRO_2$ during air inspiration and oxygen challenge.
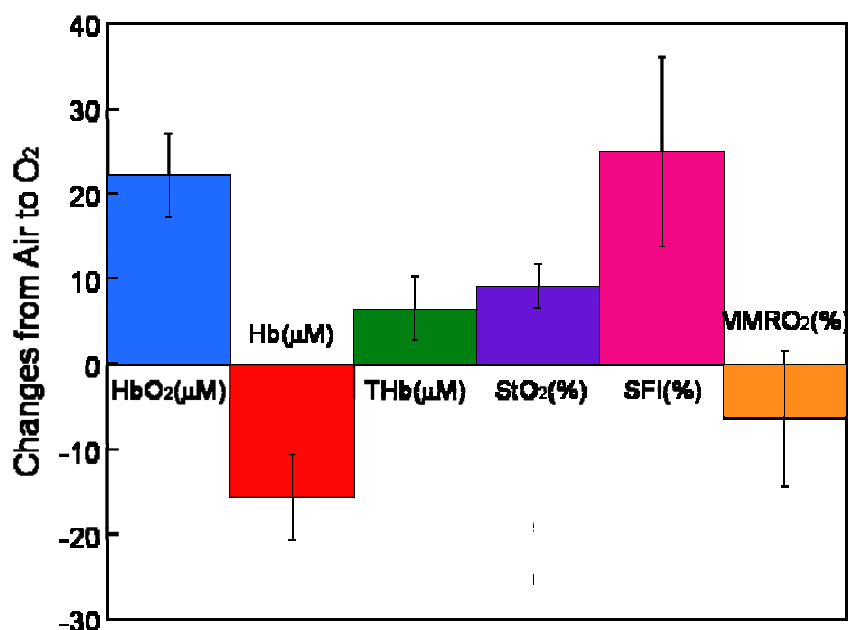

Figure 3: Bar graph of the change in tissue chromophores, speckle flow index, and mammary metabolic rate of oxygen

4. DISCUSSION

In general, an increase in the change of HbO_2 and S_tO_2 as well as a decrease in the change Hb is observed during oxygen challenge, as seen in both Figure 2 and Figure 3, corresponding to an increase in the change in blood perfusion (SFI) and decrease in the change of $MMRO_2$. In addition, there is a strong positive correlation between the change in HbO_2 and S_tO_2 and change in blood perfusion during oxygen challenge. Correspondingly, there is a strong negative correlation between decreases in the change in Hb concentration and increases in the change in blood perfusion. An interesting observation is that there does not appear to be any correlation between changes in total hemoglobin concentration and

changes in SFI values. This observation bears further investigation as it potentially may provide insight into the relationship between blood perfusion and blood content.

We have shown that our novel WiFI system has the potential to monitor tumor metabolic changes during hyperoxic respiratory challenge. The information obtained from this study can potentially give further insight into relationships between blood perfusion and corresponding changes in tissue chromophore concentration. Future work includes continuing these measurements on more tumors and determining the interplay between each of these tumor metabolic markers.

REFERENCES

1. Jain RK, "Normalizing Tumor Vasculature with Anti-Angiogenic Therapy: A New Paradigm for Combination Therapy," Nature Medicine 7, 987-989 (2001).

2. Hou H, Lariviere JP, Demidenko E, Gladstone D, Swartz H, Khan N, "Repeated tumor pO(2) measurements by multi-site EPR oximetry as a prognostic marker for enhanced therapeutic efficacy of fractionated radiotherapy," Radiotherapy and Oncology (2008) [Epub ahead of print].

3. Cuccia DJ, Bevilacqua F, Durkin AJ, Tromberg BJ, "Modulated imaging: quanititative analysis and tomography of turbid media in the spatial-frequency domain," Optics Letters 30(11), 1354-1356 (2005).

4. Choi B, Kang NM, Nelson JS, "Laser speckle imaging for monitoring blood flow dynamics in the in vivo rodent dorsal skin fold model," Microvascular Research 68(2), 143-146 (2004).

5. Huang YC, Ringold TL, Nelson JS, Choi B, "Noninvasive blood flow imaging for real-time feedback during laser therapy of port wine stain birthmarks," Lasers in Surgery and Medicine 40(3), 167-173 (2008).

6. Shafee N, Smith CR, Wei S, Kim Y, Mills GB, Hortobagyi GN, Stanbridge EJ, Lee EY, "Cancer stem cells contribute to cisplatin resistance in Brca1/p53-mediated mouse mammary tumors, "Cancer Research 68(9), 3243-50 (2008).

7. Zhou C, Choe R, Shah N, Durduran T, Yu G, Durkin A, Hsiang D, Mehta R, Butler J, Cerussi A, Tromberg BJ, Yodh AG., "Diffuse optical monitoring of blood flow and oxygenation in human breast cancer during early stages of neoadjuvant chemotherapy," Journal of Biomedical Optics 12(5), 051903 (2007).